



Cite this: *Nanoscale Adv.*, 2021, **3**, 3537

## The interaction of size-selected $\text{Ru}_3$ clusters with RF-deposited $\text{TiO}_2$ : probing Ru–CO binding sites with CO-temperature programmed desorption†

Liam Howard-Fabretto,<sup>ab</sup> Timothy J. Gorey,<sup>c</sup> Guangjing Li,<sup>c</sup> Siriluck Tesana,<sup>d</sup> Gregory F. Metha,<sup>de</sup> Scott L. Anderson<sup>ID c</sup> and Gunther G. Andersson<sup>ID \*ab</sup>

Small Ru clusters are efficient catalysts for chemical reactions such as CO hydrogenation. In this study 3-atom  $\text{Ru}_3$  clusters were deposited onto radio frequency (RF)-deposited  $\text{TiO}_2$  which is an inexpensive, nanoparticulate form of  $\text{TiO}_2$ .  $\text{TiO}_2$  substrates are notable in that they form strong metal–substrate interactions with clusters. Using temperature programmed desorption to probe Ru–CO binding sites, and X-ray photoelectron spectroscopy to provide chemical information on clusters, differences in cluster–support interactions were studied for  $\text{Ru}_3$  deposited using both an ultra-high vacuum cluster source and chemical vapour deposition of  $\text{Ru}_3(\text{CO})_{12}$ . The  $\text{TiO}_2$  was treated with different  $\text{Ar}^+$  sputter doses prior to cluster depositions, and  $\text{SiO}_2$  was also used as a comparison substrate. For cluster source-deposited  $\text{Ru}_3$ , heating to 800 K caused cluster agglomeration on  $\text{SiO}_2$  and oxidation on non-sputtered  $\text{TiO}_2$ . For cluster source-deposited  $\text{Ru}_3$  on sputtered  $\text{TiO}_2$  substrates, all Ru–CO binding sites were blocked as-deposited and it was concluded that for the binding sites to be preserved for potential catalytic benefit, sputtering of  $\text{TiO}_2$  before cluster deposition cannot be applied. Conversely, for  $\text{Ru}_3(\text{CO})_{12}$  on sputtered  $\text{TiO}_2$  the clusters were protected by their ligands and Ru–CO binding sites were only blocked once the sample was heated to 723 K. The mechanism for complete blocking of CO sites on sputtered  $\text{TiO}_2$  could not be directly determined; however, comparisons to the literature indicate that the likely reasons for blocking of the CO adsorption sites are encapsulation into the  $\text{TiO}_x$  layer reduced through sputtering and also partial oxidation of the Ru clusters.

Received 10th March 2021  
Accepted 17th April 2021

DOI: 10.1039/d1na00181g  
[rsc.li/nanoscale-advances](http://rsc.li/nanoscale-advances)

## Introduction

Metal clusters are generally defined as groups of metal atoms with sizes less than  $\sim 300$  atoms.<sup>1–6</sup> They often possess unique electronic and catalytic properties which are highly tuneable, such that the addition or subtraction of just one atom to a small cluster can be a deciding factor on whether it functions as a catalyst or not.<sup>7</sup> For this reason, experiments often focus on a single cluster size. Ru clusters in particular have been shown

to be among the most active catalysts for industrial and environmentally relevant reactions such as CO and  $\text{CO}_2$  hydrogenation.<sup>8–17</sup> Two of the main ways to deposit Ru clusters onto substrates is through the preparation of bare clusters in vacuum using an ultra-high vacuum (UHV) cluster source, or through depositing ligand-stabilized clusters such as  $\text{Ru}_3(\text{CO})_{12}$  using chemical vapour deposition (CVD)<sup>18–22</sup> or a solution-based deposition.<sup>23</sup> This process of depositing metal carbonyl compounds using CVD is well explored in the literature and has been used to deposit clusters onto a number of substrates such as; metals (*e.g.* Au), metal oxides (*e.g.*  $\text{TiO}_2$ ), non-metal oxides (*e.g.*  $\text{SiO}_2$ ) and others such as zeolites.<sup>19,24–29</sup> When depositing ligand-stabilized clusters, extra post-deposition surface treatments such as heating are needed to remove the ligands if bare metal clusters are desired on the substrate.

$\text{TiO}_2$  is a photocatalytically active substrate<sup>30</sup> and is a common choice as a substrate for the deposition of clusters.<sup>19,20,31–43</sup> Here we used RF-deposited  $\text{TiO}_2$  as a substrate. It is a nanoparticulate form of  $\text{TiO}_2$  made by radio frequency (RF) sputtering a  $\text{TiO}_2$  wafer onto a substrate (sputter deposition) under UHV, in the present case  $\text{Si}(100)$ . This process produces a dense, uniform, stoichiometry-controlled layer of  $\text{TiO}_2$  more cheaply and readily than  $\text{TiO}_2(110)$ .<sup>44</sup> RF-deposited  $\text{TiO}_2$  is

<sup>a</sup>Flinders Institute for Nanoscale Science and Technology, Flinders University, Adelaide, South Australia 5042, Australia. E-mail: gunther.andersson@flinders.edu.au

<sup>b</sup>Flinders Microscopy and Microanalysis, College of Science and Engineering, Flinders University, Adelaide, South Australia 5042, Australia

<sup>c</sup>Chemistry Department, University of Utah, 315 S. 1400 E., Salt Lake City, UT 84112, USA

<sup>d</sup>The MacDiarmid Institute for Advanced Materials and Nanotechnology, School of Physical and Chemical Sciences, University of Canterbury, Christchurch 8141, New Zealand

<sup>e</sup>Department of Chemistry, University of Adelaide, Adelaide, South Australia 5005, Australia

† Electronic supplementary information (ESI) available. See DOI: [10.1039/d1na00181g](https://doi.org/10.1039/d1na00181g)



polycrystalline and does not have a surface as flat as a single crystal. RF-deposited  $\text{TiO}_2$  does, however, more closely reflect the situation of  $\text{TiO}_2$  as used in a real catalyst than single crystal samples. Our previous studies have shown RF-deposited  $\text{TiO}_2$  does not feature X-ray diffraction peaks related to a specific crystal phase prior to heat treatment, however heating under vacuum or atmosphere results in anatase phase formation, and strong heating to 1373 K for 18 hours under atmosphere results in the emergence of a rutile crystal peak in addition to anatase.<sup>45</sup>

A key problem of clusters deposited onto surfaces is maintaining the properties of size-selected clusters by preventing them from agglomeration, in particular at elevated temperatures.<sup>46</sup> One method to help with this is to induce defects on the substrate surface prior to cluster deposition.<sup>47,48</sup> Clusters are known to preferentially bind to defect sites, as their surface energy is greater than the corresponding perfect crystal structure.<sup>48</sup> As a specific example regarding  $\text{TiO}_2$  substrates, a study by Krishnan *et al.*<sup>48</sup> showed that for  $\text{Au}_9$  clusters supported on atomic layer deposited (ALD)  $\text{TiO}_2$ , sputter-treating the surface with  $\text{Ar}^+$  prior to cluster deposition was able to help prevent cluster agglomeration. The anchoring of clusters to defect sites on  $\text{TiO}_2$  has also been demonstrated by DFT calculations of  $\text{Au}$  clusters on  $\text{TiO}_2(110)$ .<sup>49</sup> However, the cluster–substrate interaction, and therefore agglomeration characteristics, will be different for each cluster/substrate combination.

There are two main types of defects: oxygen vacancies and interstitial titanium ions<sup>30</sup> both resulting in the presence of  $\text{Ti}^{3+}$  in the  $\text{TiO}_2$ . The transport of each in the substrate can be explained by vacancy and interstitial models respectively.<sup>30,50–52</sup> Interstitials are atoms present within crystal lattice locations where they should not normally be present.  $\text{Ar}^+$  sputter treatment of  $\text{TiO}_2$  removes  $\text{O}$  atoms more preferentially than  $\text{Ti}$  atoms from the surface, and the main surface defect sites from sputtering are predominantly vacancies in the bridging oxygen rows of the  $\text{TiO}_2$ .<sup>30,53</sup> These defect sites act as electron donors to clusters because the oxygen removal leaves behind two electrons which previously occupied  $\text{O}_{2p}$  valence band levels.<sup>30,54</sup>

Previous studies on the effects of heating systems of small, size-selected Ru clusters on  $\text{TiO}_2$  have often focussed on Ru deposited using  $\text{Ru}_3(\text{CO})_{12}$ : two separate studies by Zhao *et al.* and Rizzi *et al.*<sup>18,19</sup> have been performed on  $\text{Ru}_3(\text{CO})_{12}$  deposited by CVD onto  $\text{TiO}_2(110)$ , using X-ray photoelectron spectroscopy (XPS) and/or CO-temperature programmed desorption (CO-TPD). Both studies found that there is partial decomposition of  $\text{Ru}_3(\text{CO})_{12}$  when deposited onto room-temperature  $\text{TiO}_2(110)$ .<sup>18,19</sup> Furthermore, Zhao *et al.*<sup>19</sup> demonstrated using XPS and TPD that heating to 700 K under UHV yielded almost pure Ru particles on the surface, but heating to 600 K while dosing  $\text{O}_2$  resulted in oxidised Ru. The latter point was also supported in the Rizzi *et al.* study using XPS.<sup>18</sup> The specific cluster–substrate interaction can have a large effect on the state of supported clusters, even for differing forms of  $\text{TiO}_2$ ; CO-TPD spectra have been shown to have different CO desorption features for  $\text{Ru}_3(\text{CO})_{12}$  deposited onto varying forms of  $\text{TiO}_2$ , such as  $\text{TiO}_2(110)$ ,<sup>19</sup> polycrystalline P25  $\text{TiO}_2$ ,<sup>23</sup> and  $\text{TiO}_2/\text{Mo}(110)$ .<sup>20</sup> Other studies have used differing Ru/ $\text{TiO}_2$  systems with different thermal stability results, including one study by

Komaya *et al.*<sup>55</sup> for large Ru particles deposited with  $\text{Ru}(\text{NO})(\text{NO}_3)_3$  onto P25 nanocrystalline  $\text{TiO}_2$ , where heating to 573 K resulted in the encapsulation of Ru by an amorphous titania layer. These studies show that it is unclear how Ru clusters interact with the substrate when deposited onto titania, in particular when heating of the cluster/substrate system is involved. It is therefore important to test the interaction and stability of Ru clusters on RF-deposited  $\text{TiO}_2$  because studies performed on differing  $\text{TiO}_2$  forms cannot predict the results for this substrate. Of particular interest is agglomeration of the clusters and encapsulation into the substrate.

The aim of this study was to determine whether defects induced in RF-deposited  $\text{TiO}_2$  substrates help to avoid agglomeration of bare  $\text{Ru}_3$  and  $\text{Ru}_3(\text{CO})_{12}$  clusters upon deposition, and how the clusters interact with  $\text{TiO}_2$  substrates upon heating to  $\sim 800$  K. The clusters were deposited both from a cluster source (bare  $\text{Ru}_3$ ) and evaporation of  $\text{Ru}_3(\text{CO})_{12}$  via chemical vapour deposition (CVD). To the knowledge of the authors no previous studies exist for size-selected Ru deposited by a cluster source onto  $\text{TiO}_2$ , and thus comparison between the results of these two common deposition methods is of critical importance. CO-TPD is used to probe the available CO adsorption sites on the metal clusters, as well as for probing the removal of ligands with heating in the case of CO-stabilized clusters.<sup>19,20,56–60</sup> XPS is used to analyse the composition of the surface and to determine concentration depth profiles.

## Methodology

### Materials

P-type, boron-doped Si(100) wafers were purchased from MTI Corporation and used without further modification. RF-deposited  $\text{TiO}_2$  substrates (referred to as  $\text{TiO}_2$ ) were prepared by RF magnetron-sputtering using a 99.9% pure  $\text{TiO}_2$  ceramic target, where  $\text{TiO}_2$  is deposited *via* sputtering of the target onto a substrate, in this case a Si(100) wafer. This was under high vacuum using an HHV/Edwards TF500 Sputter Coater at a pressure  $<2 \times 10^{-5}$  mbar, using 10 sccm Ar for sputtering the  $\text{TiO}_2$  surface. The power was ramped up at 50 W per minute to 500 W, and a shutter was then removed from the target for 50 minutes, allowing the deposition of material onto the rotating wafer. The thickness of the  $\text{TiO}_2$  was approximately 150 nm, which is thick enough that the  $\text{SiO}_2$  wafer beneath would not be detectable in the electron spectra. This thickness was estimated based on SEM measurements previously performed on wafers prepared using similar methodology on the same apparatus.<sup>45</sup>

Clusters were prepared by depositions using (i) chemical vapour deposition (CVD) of ligated clusters and (ii) depositing bare clusters from a gas phase cluster source (CS). CVD depositions were performed with  $\text{Ru}_3(\text{CO})_{12}$ ; this was prepared as a powdered sample, according to synthesis procedures reported by Faure *et al.*<sup>61</sup> CVD depositions were performed under UHV in a separate instrument for CO-TPD and XPS analysis. CS depositions were performed by a laser ablation cluster source which has been used and described in several previous publications.<sup>58,60,62</sup> For cluster source-deposition of bare  $\text{Ru}_3$  clusters, the source was a 99.9% pure target of Ru.



## Substrates and samples

$\text{Ru}_3$  was deposited onto four different types of substrates: two  $\text{TiO}_2$  substrates modified by  $\text{Ar}^+$  sputter treatment (prior to the deposition of Ru clusters) at two different  $\text{Ar}^+$  doses, non-sputtered  $\text{TiO}_2$ , and non-sputtered  $\text{SiO}_2$  for comparison. The different sputter dosages for  $\text{TiO}_2$  have been designated as follows: “low-dose sputtered  $\text{TiO}_2$ ” was treated with  $4 \times 10^{13} \text{ Ar}^+/\text{cm}^2$ , and “high-dose sputtered  $\text{TiO}_2$ ” was treated with  $6 \times 10^{14} \text{ Ar}^+/\text{cm}^2$ . Additionally, a “non-sputtered  $\text{TiO}_2$ ” sample was used. In the text these will be abbreviated to LDS- $\text{TiO}_2$ , HDS- $\text{TiO}_2$ , and NS- $\text{TiO}_2$ , respectively. A list of the substrates and their abbreviated names are given in Table 1. Deposition of  $\text{Ru}_3$  from CS was performed on all 4 substrates. However, deposition of  $\text{Ru}_3(\text{CO})_{12}$  from CVD was only undertaken on an HDS- $\text{TiO}_2$  substrate. Clusters deposited by CS will herein be referred to as “ $\text{Ru}_3$ ”, while clusters deposited by CVD will be referred to as “ $\text{Ru}_3(\text{CO})_{12}$ ”. 5 samples were analysed with CO-TPD overall, and blank measurements CO-TPD were performed prior to the deposition of Ru clusters. Additional samples were prepared for further XPS analysis, and thus the XPS measurements in some cases were of samples prepared with an identical method, rather than the same sample as was analysed with CO-TPD. A list of all samples analysed is given in the ESI (Table S1†).

## Instrumentation

CS depositions, as well as XPS, CO-TPD, and  $\text{Ar}^+$  sputter treatment were performed using a UHV apparatus with a main chamber base pressure of  $<2 \times 10^{-10} \text{ mbar}$  at the University of Utah. All CS measurements and analysis were performed on this apparatus (*i.e.* all measurements except CVD depositions and the XPS of metallic Ru reference material, which are described separately). Samples were stored in the main chamber when depositing clusters using the cluster source. The instrument featured liquid  $\text{N}_2$  cooling and resistive heating. A C-type thermocouple was spot welded to the backing plate of the sample holder to monitor the temperature. The instrument includes capabilities for continuous temperature control and automatic, linear temperature ramping, and soft landing of small metal clusters. A soft-landing deposition energy of  $\sim 1 \text{ eV}$  per atom was used for the  $\text{Ru}_3$  clusters. Previous studies of the deposition of small Ir clusters onto  $\text{TiO}_2$  and  $\text{SiO}_2$  showed that impact energies in the tens of eV per atom are required to embed the clusters into these substrates (*e.g.* at least 10 eV per atom for small Ir clusters on  $\text{TiO}_2$ ).<sup>63,64</sup> Thus, the  $\sim 1 \text{ eV}$  per atom deposition energy is considered suitable to not cause Ru cluster

damage or embedding during depositions. Further details on the CS instrument and depositions are provided in the ESI.†

The chemical vapor deposition (CVD) of ligated  $\text{Ru}_3(\text{CO})_{12}$  clusters was performed using a UHV apparatus at Flinders University in Adelaide. The substrates were prepared in a main chamber featuring a base pressure of  $<2 \times 10^{-10} \text{ mbar}$ , which included electron bombardment heating and  $\text{Ar}^+$  sputter treatment. Chemical vapour depositions (CVD) of ligated  $\text{Ru}_3(\text{CO})_{12}$  clusters were performed *ex situ* in a separate loading chamber, with a base pressure of  $<8 \times 10^{-8} \text{ mbar}$ . Further details on the CVD process are provided in the ESI.† These samples were transported from Flinders University to the University of Utah for CO-TPD analysis.

The Utah and Adelaide instruments use different sputter guns; the substrates for the CVD sample (Adelaide) was prepared using 3 keV  $\text{Ar}^+$ , while the substrates for the CS samples (Utah) were prepared using 2 keV  $\text{Ar}^+$ . The defects may extend deeper into the bulk for the CVD sample due to the higher  $\text{Ar}^+$  impact energy.<sup>33,34</sup> This was not corrected for, and a slight variation in defects on the substrate was deemed not to be of critical importance for this experiment.

## CO-temperature programmed desorption (CO-TPD)

CO-TPD is used to investigate the desorption of CO molecules from the various samples. CO molecules are typically first dosed onto a sample under UHV, but the technique can also be used to analyse the de-ligation of CO-ligated clusters such as  $\text{Ru}_3(\text{CO})_{12}$ , where CO does not need to be dosed prior to measurements.<sup>12,19,20</sup> When the CO dosing and temperature ramping procedure is repeated for multiple cycles, CO-TPD can show the effect of heating on the available CO binding sites on the surface, which can give insights into cluster/substrate interactions.

For CO-TPD measurements (excluding CO de-ligation), the sample was dosed with isotopically labelled  $^{13}\text{CO}$  (mass 29) at 180 K. They were exposed to 10 L  $^{13}\text{CO}$ , which was above the saturation dose. CO exposure was through a dosing tube which terminated approximately 2 cm from the surface of the substrate; this increased the gas flux at the surface by a factor of approximately 10 compared to dosing the gas into the chamber without the tube. This increase factor was determined previously as per the method described by Kaden *et al.*<sup>56</sup>

For each substrate, CO-TPD measurements were performed before and after CS cluster depositions. After a deposition, the CO procedure was initiated as quickly as practicable possible. This is for all samples except the CVD sample which was not

**Table 1** Summary of the different supporting substrates used in this study. The designated sample names are given as well as abbreviated names for the  $\text{TiO}_2$  substrates

Substrate material	$\text{Ar}^+$ sputter dose ( $\text{Ar}^+/\text{cm}^2$ )	Designated sample name	Abbreviated name
$\text{TiO}_2$	None	Non-sputtered $\text{TiO}_2$	NS- $\text{TiO}_2$
$\text{TiO}_2$	$4 \times 10^{13}$	Low-dose sputtered $\text{TiO}_2$	LDS- $\text{TiO}_2$
$\text{TiO}_2$	$6 \times 10^{14}$	High-dose sputtered $\text{TiO}_2$	HDS- $\text{TiO}_2$
$\text{SiO}_2/\text{Si}(100)$	None	$\text{SiO}_2$	$\text{SiO}_2$



deposited *in situ*. The standard procedure for CO-TPD cycle is as follows. After CO dosing, the sample was positioned at a distance of 0.5 mm from the differentially pumped quadrupole mass spectrometer (QMS) entrance, which is a 2.5 mm diameter aperture in a skimmer cone. The temperature was then ramped at a rate of 3 K s<sup>-1</sup> from 170 K to 800 K, while masses corresponding to CH<sub>3</sub>, O, H<sub>2</sub>O, <sup>12</sup>CO, <sup>13</sup>CO, O<sub>2</sub>, <sup>12</sup>CO<sub>2</sub>, <sup>13</sup>CO<sub>2</sub> were monitored in 50 ms total cycles using a QMS made by UTI. Masses apart from <sup>12</sup>CO and <sup>13</sup>CO were only monitored for irregularities or unexpected reaction products. Between 700 K and 750 K the sample holder “degassed” CO resulting in a sharply increased background. Data points beyond this temperature and up to 800 K were therefore not considered for analysis. After the completion of a CO-TPD cycle, the sample was cooled again, and the cycle was repeated 3 to 4 times per sample. Additional details on the calibration of the QMS signal, integration of the CO-TPD spectra, and the accuracy of the measurement and calibration are provided in the ESI.†

The CO-TPD procedure for Ru<sub>3</sub>(CO)<sub>12</sub>/HDS-TiO<sub>2</sub> was slightly different; the samples were cooled to 180 K and the CO-TPD heat ramping process was initiated with no further treatment (there were no samples of Ru<sub>3</sub>(CO)<sub>12</sub> on NS-TiO<sub>2</sub> or LDS-TiO<sub>2</sub>). The clusters were already saturated with <sup>12</sup>CO ligands, and thus for the 1<sup>st</sup> cycle no <sup>13</sup>CO was dosed, and <sup>12</sup>CO was the mass of interest. As this sample had been exposed to atmosphere before measurements, there may have been a small component of the CO-TPD signal which was due to the desorption of adsorbed CO contamination. This was not corrected for but due to the large number of CO ligands measured desorbing in the 1<sup>st</sup> CO-TPD cycle, any effects from contamination were deemed minimal in comparison to the signal strength. The temperature was only ramped to 723 K on the 1<sup>st</sup> CO-TPD cycle. <sup>13</sup>CO was dosed as per the standard procedure for the CO-TPD on the 2<sup>nd</sup> and 3<sup>rd</sup> cycles. An additional complication was that on the 1<sup>st</sup> cycle the CO desorption rate reached the maximum count limit of the QMS which caused two effects; the <sup>12</sup>CO spectrum was distorted due to saturation, and the measured <sup>13</sup>CO signal clearly was actually due to overlap of the adjacent <sup>12</sup>CO mass peak signal. This detection of a small fraction of the overlapping <sup>12</sup>CO signal at mass 29 allowed us to correct the <sup>12</sup>CO spectrum for saturation by scaling the <sup>13</sup>CO spectral intensities so that they matched the <sup>12</sup>CO signal at low temperature, where the signal was well below the saturation level. Note that after the 1<sup>st</sup> TPD on the CVD sample, and in all TPD experiments with CS clusters, the <sup>12</sup>CO signal was small, and unsaturated.

## XPS methods

For XPS measurements of cluster-deposited samples (in Utah), the Ru 3d, C 1s and O 1s regions were measured for each sample, while the Ti 2p and Si 2p regions were additionally measured for TiO<sub>2</sub> and SiO<sub>2</sub> substrates, respectively. The Ru 3d and C 1s regions overlap and will be referred to as the Ru 3d/C 1s region. XPS of cluster samples was performed *in situ* (except for Ru<sub>3</sub>(CO)<sub>12</sub>/HDS-TiO<sub>2</sub>) using an Al K $\alpha$  source and 10 eV pass energy. X-ray photons were incident to the surface at 54.7°, and ejected photoelectrons were measured normal to the sample.

No evidence for charging was found for any sample. A hemispherical analyzer (HSA, Physical Electronics) was used; this featured an area-selective lens with a 1.1 mm diameter analysis area, which was optimised to measure cluster spots of 2 mm in diameter without XPS signal from the surrounding bare substrate. Binding energies were calibrated to C 1s = 285.0 eV. Details for the XPS data analysis including peak fitting, line shapes used for fitting (Table S2†) and uncertainties are provided in the ESI.†

An XPS spectrum of an Ru reference material was measured on a separate XPS instrument (in Adelaide) with a Mg K $\alpha$  excitation and a Phoibos 100 HSA (SPECS, Germany). The Ru reference sample was taken from a 99.9% pure Ru metal sample (Fig. S1, ESI†). A measurement was first performed with no surface treatment, and then again after heating to 1073 K for 10 minutes and sputtering with 3 keV Ar<sup>+</sup> for 1 hour to remove the surface Ru oxide layer and any hydrocarbon contamination. The BE scale for these measurements was calibrated to the C 1s peak for the pre-treatment XPS spectrum before hydrocarbon removal. Additionally, an *in situ* measurement of the Ru<sub>3</sub>(CO)<sub>12</sub>/HDS-TiO<sub>2</sub> was performed on the XPS same instrument before removing the sample from vacuum, to estimate the number of ligands on the clusters (results shown in ESI Table S3†).

## Results

### Temperature programmed desorption

**CO-TPD of Ru<sub>3</sub>/SiO<sub>2</sub>.** Fig. 1a shows CO-TPD measurements of blank SiO<sub>2</sub> and Ru<sub>3</sub> on SiO<sub>2</sub>. CO-temperature programmed desorption (CO-TPD) is an analysis technique useful for probing the available CO adsorption sites on metal clusters, as well as for probing the removal of ligands with heating in the case of CO-stabilized clusters.<sup>19,20,56–60</sup> When discussing peaks in CO-TPD figures, they will be labelled based on the temperature corresponding to the peak CO desorption rate. It is assumed that higher temperature peaks correspond to sites with stronger CO binding. Due to the continuous temperature ramping of the CO-TPD measurements the temperature at the peak CO desorption rate is typically greater than the minimum temperature required for CO desorption to occur for that particular binding site. SiO<sub>2</sub> was used for reference measurements because it is a nonreducible oxide substrate that is stable at the temperatures being used and does not form a strong metal support interaction (SMSI) with clusters under typical conditions.<sup>65–67</sup>

Fig. 1a shows that very little CO has desorbed from blank SiO<sub>2</sub>, with two small features centred at 210 K and 285 K. Furthermore, there was no change between the blank measurements over 3 repeated TPD cycles (traces not shown in figure), indicating the affinity of the surface for CO was not strongly affected or changed by heating to 800 K. The 1<sup>st</sup> CO-TPD cycle for Ru<sub>3</sub>/SiO<sub>2</sub> features a small peak at 210 K, which is related to desorption of CO from the SiO<sub>2</sub> substrate. The remaining features in the spectrum are due to CO desorbing from Ru-CO binding sites. Notably, there is a small peak at 260 K and then a large, main desorption peak at 530 K. In this study, these two features will be treated as the reference Ru-CO



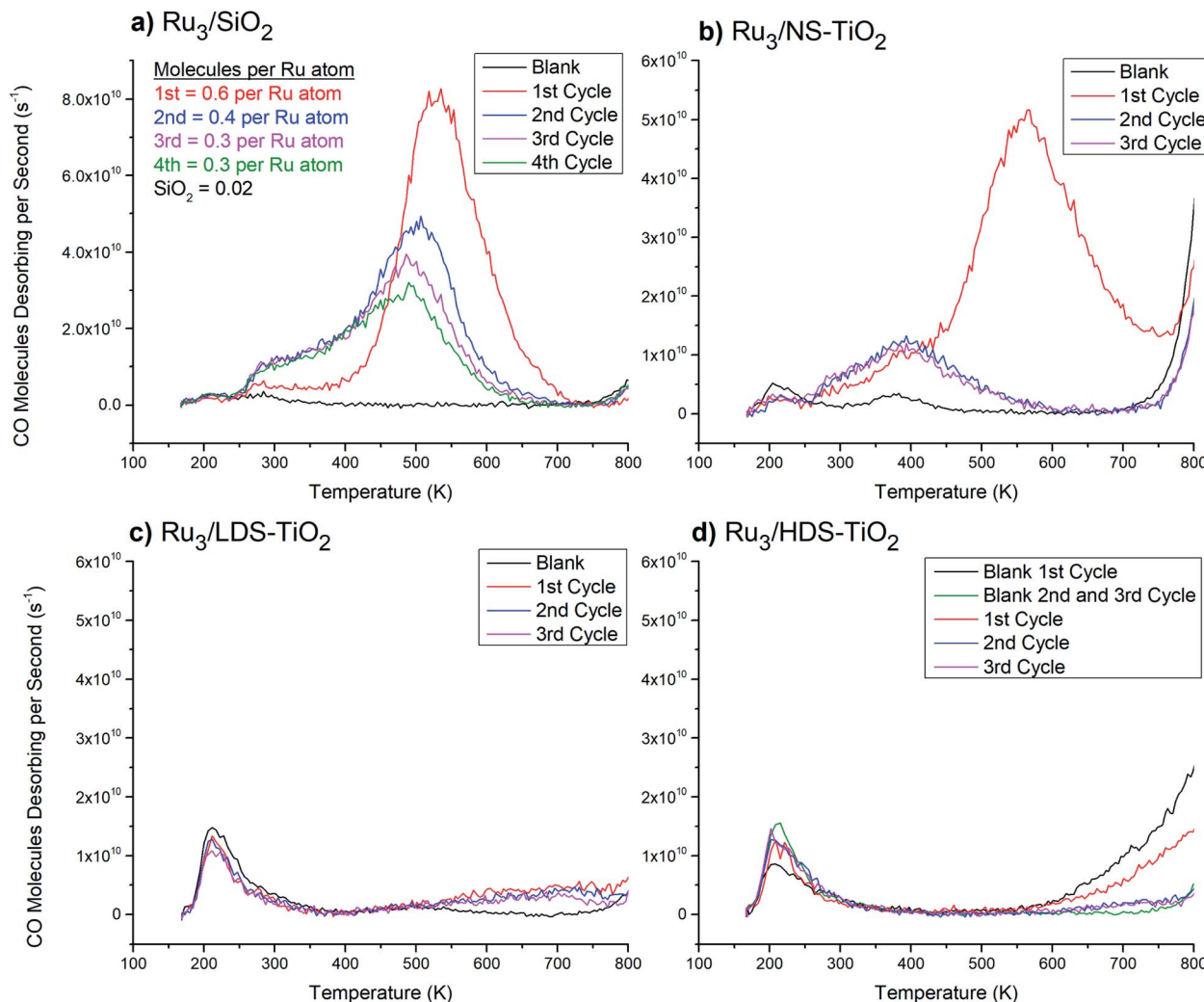


**Fig. 1**  $^{13}\text{CO}$ -TPD from  $\text{Ru}_3$  CS-deposited onto various substrates. Blank measurements were performed before  $\text{Ru}_3$  deposition, and the spectra are averages of 3 blank cycles each where there were no noticeable changes (except for (d), discussed below). (a)  $\text{Ru}_3/\text{SiO}_2$ . Quantification of CO molecules desorbing per Ru atom is shown in the top left corner. For comparison purposes the quantified blank  $\text{SiO}_2$  desorption assumes the same number of Ru atoms were deposited as the cluster-loaded measurements. The uncertainty of CO molecules desorbing per atom is  $\sim 50\%$  (see ESI†). (b)  $\text{Ru}_3/\text{NS-TiO}_2$ . (c)  $\text{Ru}_3/\text{LDS-TiO}_2$ . (d)  $\text{Ru}_3/\text{HDS-TiO}_2$ . For HDS-TiO<sub>2</sub> two blank measurements are shown: the 1<sup>st</sup> cycle and an average of the 2<sup>nd</sup> and 3<sup>rd</sup> cycles. There was presumably a change in the blank spectrum after the 1<sup>st</sup> cycle because the HDS-TiO<sub>2</sub> blank featured more hydrocarbons adsorbed from the vacuum before the CO-TPD cycle, resulting from defected TiO<sub>2</sub> being more reactive than pristine TiO<sub>2</sub>.<sup>30</sup>

desorption peaks for CO desorbing from supported Ru clusters which have not chemically reacted with the substrate or formed an SMSI state. In the 2<sup>nd</sup> to 4<sup>th</sup> cycles, the 260 K desorption feature increased in size (Fig. 1a). Also, the larger high temperature CO peak changed shape with successive CO-TPD cycles by decreasing in size and shifting to lower temperatures. By the 4<sup>th</sup> cycle the main desorption peak was at 500 K, and the total number of CO molecules desorbing had decreased to half the value in the 1<sup>st</sup> cycle.

**CO-TPD of  $\text{Ru}_3/\text{TiO}_2$ .** Fig. 1b-d shows the CO-TPD of  $\text{Ru}_3$  on the three TiO<sub>2</sub> substrates; (b) NS-TiO<sub>2</sub>, (c) LDS-TiO<sub>2</sub> and (d) HDS-TiO<sub>2</sub>. For each substrate, a “Blank” CO-TPD measurement with no clusters was also performed for 3 cycles, which are shown as average spectra in the figures. For the NS-TiO<sub>2</sub> substrate (Fig. 1b), the blank measurement shows 2 desorption features at

210 K and 380 K. The 1<sup>st</sup> CO-TPD cycle for the cluster-loaded  $\text{Ru}_3/\text{NS-TiO}_2$  features a similar CO-TPD spectrum to the 1<sup>st</sup> cycle on  $\text{SiO}_2$  (Fig. 1a). The peak at 180 K was still present when  $\text{Ru}_3$  clusters were deposited onto the TiO<sub>2</sub> substrate but was reduced in size by approximately half. This was a result of the  $\text{Ru}_3$  binding to, and covering, these low temperature CO binding sites on the substrate. In addition, a shoulder peak at 380 K and a large desorption peak at 560 K (the main peak) now appear. These appeared to be shifted versions of the 260 K and 530 K peaks present for the  $\text{Ru}_3/\text{SiO}_2$  sample.

The 2<sup>nd</sup> and 3<sup>rd</sup> heating cycles for  $\text{Ru}_3/\text{NS-TiO}_2$  (Fig. 1b) have a consistent CO desorption shape which is different to that of the 1<sup>st</sup> cycle. They still have the 380 K feature from the 1<sup>st</sup> cycle, with a slightly increased height and width, but the 560 K main desorption peak has been completely removed. Thus, heating to

800 K caused the loss of the most strongly-binding and most numerous CO binding site on the Ru clusters. The increase in desorption of the 380 K peak after heating was not proportional to the loss in signal of the 560 K peak, indicating that after heating there were fewer CO binding sites available overall. The changes in the CO-TPD spectra cannot be associated with cluster agglomeration alone, because the result would be a CO desorption shape more like that of  $\text{Ru}_3/\text{SiO}_2$  on the 2<sup>nd</sup> to 4<sup>th</sup> CO-TPD cycles (Fig. 1a), where agglomeration occurred but the peak was not lost completely. As such, agglomeration was ruled out as the sole cause for the change in CO desorption after the 1<sup>st</sup> cycle. The XPS results for the XPS samples provided further insights into the loss of the main desorption peak, by providing evidence that heating to 800 K caused a change in oxidation state of the clusters. It is likely that the clusters were oxidised by the surface when heated, which blocked the main Ru-CO binding site. This is discussed further in detail below. Some agglomeration may have also contributed to the loss of the peak, which cannot be ruled out with this data.

The blank CO-TPD spectra for the sputtered substrates, namely LDS-TiO<sub>2</sub> and HDS-TiO<sub>2</sub> (Fig. 1c and d respectively) feature one main peak at 210 K, which was larger than that for the blank NS-TiO<sub>2</sub> (Fig. 1b). Because the CO desorption rate for the 210 K peak increased for sputtered TiO<sub>2</sub>, it is likely that this peak was related to CO adsorbed to defected surface regions on the blank TiO<sub>2</sub>. The second, 380 K peak present for the blank NS-TiO<sub>2</sub> was not present on blank LDS-TiO<sub>2</sub> or HDS-TiO<sub>2</sub>; however, the blank LDS-TiO<sub>2</sub> spectrum has a second, wider desorption feature at 500 K which may be a shifted version of the 380 K peak seen for the blank NS-TiO<sub>2</sub> sample (Fig. 1b). For the blank HDS-TiO<sub>2</sub> spectrum (Fig. 1d) there is no such desorption feature, which may indicate the 380 K feature for blank NS-TiO<sub>2</sub> was from CO binding sites on non-defected, pristine TiO<sub>2</sub> regions, and the binding site was modified by sputtering (for LDS-TiO<sub>2</sub>) before being lost completely at a higher sputter dosage (for HDS-TiO<sub>2</sub>).

The CO-TPD spectrum for the  $\text{Ru}_3/\text{LDS-TiO}_2$  sample (Fig. 1c) features a broad CO desorption peak for all cycles which was not seen for the blank sample, with deviation from blank at 550 K. For  $\text{Ru}_3/\text{HDS-TiO}_2$  (Fig. 1d) there was a similar deviation from the blank sample above 550 K, although the exact shape was not the same. None of the characteristic CO desorption features seen in the  $\text{Ru}_3/\text{SiO}_2$  sample were present for Ru<sub>3</sub> on either sputtered TiO<sub>2</sub> substrate. This means the clusters were interacting with the sputtered TiO<sub>2</sub> in such a way that all Ru-CO binding sites were blocked, both before and after the sample was heated for CO-TPD. Although agglomeration and/or oxidation may have contributed to the loss of Ru-CO binding sites, the complete loss of all sites suggests a different mechanism for the blocking of sites on LDS-TiO<sub>2</sub> and HDS-TiO<sub>2</sub> substrates. The cause of site-blocking for these samples was most likely that the clusters were not present on the outermost layer of the sample. This is expanded upon in detail in the Discussion section. There was good repeatability between the three CO-TPD cycles for both  $\text{Ru}_3/\text{LDS-TiO}_2$  and  $\text{Ru}_3/\text{HDS-TiO}_2$ , showing the resultant Ru/TiO<sub>2</sub> systems were stable and not changed significantly by heating to 800 K.

**CO-TPD of  $\text{Ru}_3(\text{CO})_{12}/\text{HDS-TiO}_2$ .** The 1<sup>st</sup> cycle CO-TPD desorption shape for  $\text{Ru}_3(\text{CO})_{12}/\text{HDS-TiO}_2$  (Fig. 2) features a smaller peak at 300 K and a larger peak at 600 K. The CO-TPD shape is very similar to the 1<sup>st</sup> cycle of both  $\text{Ru}_3/\text{SiO}_2$  (Fig. 1a) and  $\text{Ru}_3/\text{NS-TiO}_2$  (Fig. 1b). The peak CO desorption rate from the 1<sup>st</sup> cycle in Fig. 2 is  $6.0 \times 10^{11}$  molecules per s, which is  $\sim 12$  times greater than that of  $\text{Ru}_3/\text{NS-TiO}_2$ , which had a maximum of  $5.2 \times 10^{10}$  molecules per s (Fig. 1b), and  $\sim 7$  times greater than  $\text{Ru}_3/\text{SiO}_2$  which had a maximum of  $8.3 \times 10^{10}$  molecules per s (Fig. 1a). This higher desorption rate must be due to a greater number of CO molecules bound per Ru atom on the ligated clusters, in addition to a  $\sim 3$  times greater surface coverage for the  $\text{Ru}_3(\text{CO})_{12}$  sample. This was determined according to XPS atomic concentrations (at%) shown in Table 3 in the XPS results (*vide infra*). For the 2<sup>nd</sup> and 3<sup>rd</sup> cycles, the shape and intensity of the <sup>13</sup>CO desorption changes significantly from <sup>12</sup>CO in the 1<sup>st</sup> cycle (Fig. 2), and has a shape unique from that of the earlier CS-deposited samples. No characteristic Ru-CO binding sites are present which indicates the Ru-CO sites are being blocked, but there is a broad CO desorption peak from 180 K to 650 K, which retains the same shape and intensity between the 2<sup>nd</sup> and 3<sup>rd</sup> cycle. The similarity of the CO-TPD spectrum of the first cycle  $\text{Ru}_3(\text{CO})_{12}/\text{HDS-TiO}_2$  and the first cycle  $\text{Ru}_3/\text{SiO}_2$  suggests that the  $\text{Ru}_3(\text{CO})_{12}$  clusters do not agglomerate upon deposition onto TiO<sub>2</sub>.

There are differences between the 1<sup>st</sup> cycle CO desorption spectra of  $\text{Ru}_3(\text{CO})_{12}/\text{HDS-TiO}_2$  (Fig. 2) and the 1<sup>st</sup> cycle spectra of the previously discussed CS-deposited samples;  $\text{Ru}_3/\text{SiO}_2$  (Fig. 1a) and  $\text{Ru}_3/\text{NS-TiO}_2$  (Fig. 1b). The  $\text{Ru}_3(\text{CO})_{12}/\text{HDS-TiO}_2$  sample low temperature peak was at 300 K, while  $\text{Ru}_3/\text{SiO}_2$  and  $\text{Ru}_3/\text{NS-TiO}_2$  featured desorption peaks at 260 K and 380 K, respectively. Another difference between the 1<sup>st</sup> cycle CO-TPD spectra of the samples is the temperatures of the main, higher-temperature desorption peaks: 600 K for  $\text{Ru}_3(\text{CO})_{12}/\text{HDS-TiO}_2$ , 560 K for  $\text{Ru}_3/\text{NS-TiO}_2$ , and 530 K for  $\text{Ru}_3/\text{SiO}_2$ . This

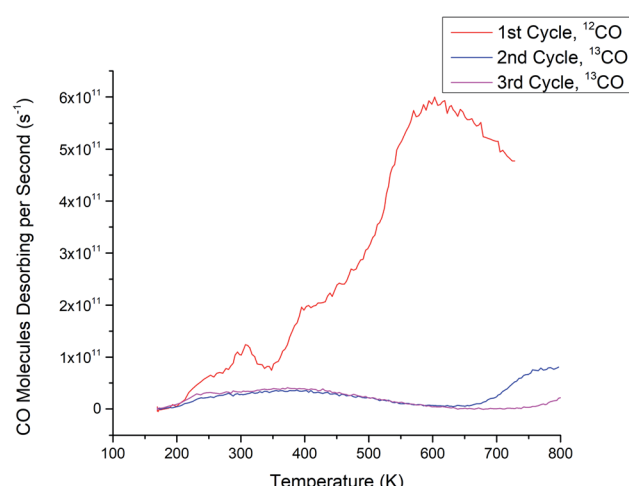


Fig. 2 CO-TPD for  $\text{Ru}_3(\text{CO})_{12}/\text{HDS-TiO}_2$ . The <sup>12</sup>CO spectrum (CO ligands) is shown for the 1<sup>st</sup> cycle and <sup>13</sup>CO spectra (*in situ* dosed CO) are shown for the 2<sup>nd</sup> and 3<sup>rd</sup> cycles. <sup>13</sup>CO was only dosed in vacuum for the 2<sup>nd</sup> and 3<sup>rd</sup> cycles.



indicates that although the Ru–CO binding sites were similar in these cases, the highest binding energy site was strongest for  $\text{Ru}_3(\text{CO})_{12}/\text{HDS-TiO}_2$ , followed by  $\text{Ru}_3/\text{TiO}_2$ , then  $\text{Ru}_3/\text{SiO}_2$ . However, the main peak starts at  $\sim 400$  K for each of these samples, and because the  $\text{Ru}_3(\text{CO})_{12}/\text{HDS-TiO}_2$  sample extends to the highest temperature this may indicate it has a slightly wider range of binding sites with differing energies that were not individually resolved in the spectra. The difference in peak desorption temperatures for the large peak between the samples may be due to a combination of multiple effects. Firstly, the direct contact of clusters to the substrate for the bare  $\text{Ru}_3$  may alter the electron density in the clusters and weaken the bond with CO compared to the ligated sample. Secondly, this could be due to less CO binding to the bare CS clusters, which affects the Ru–CO binding energy. Lastly, because  $\text{Ru}_3/\text{SiO}_2$  had the lowest peak temperature, it follows that the strong interaction between  $\text{Ru}_3$  and  $\text{TiO}_2$  stabilised the Ru–CO bonding when compared to the less strongly interacting  $\text{SiO}_2$  substrate.

A key difference comparing the full set of CO-TPD cycles for  $\text{Ru}_3(\text{CO})_{12}/\text{HDS-TiO}_2$  (Fig. 2) to  $\text{Ru}_3$  on sputtered  $\text{TiO}_2$  ( $\text{Ru}_3/\text{LDS-TiO}_2$  and  $\text{Ru}_3/\text{HDS-TiO}_2$ , see Fig. 1) was that for the bare CS samples, Ru–CO binding sites were completely blocked for the as-deposited samples, but for  $\text{Ru}_3(\text{CO})_{12}$  the sample needed to be heated in the CO-TPD procedure before Ru–CO sites were blocked. It would appear that the CO ligands on  $\text{Ru}_3(\text{CO})_{12}$  prevented the Ru–CO sites from being blocked by the HDS-TiO<sub>2</sub> substrate until the ligands were removed by the heating process during the 1<sup>st</sup> CO-TPD cycle. That is to say, the cluster–substrate interaction which blocks the Ru–CO sites does not preferentially replace ligands which are already present on the clusters. The mechanism for this site blocking is discussed below in detail together with the CS-deposited samples. Since the clusters will pin to the defect sites on sputtered  $\text{TiO}_2$ ,<sup>48,49</sup> these ligated Ru clusters were likely to be well-pinned to the substrate and present as unique,

monodispersed cluster complexes before the ligands were removed due to heating. An additional difference is that the  $\text{Ru}_3(\text{CO})_{12}/\text{HDS-TiO}_2$  was the only sample deposited *ex situ* and exposed to atmosphere. This caused the passivation of defect states in the titania due to interaction with atmospheric gasses (shown and discussed below in the XPS Results section). This most likely accounts for the differences in shape between the 2<sup>nd</sup> and 3<sup>rd</sup> cycle CO-TPD spectra between  $\text{Ru}_3/\text{HDS-TiO}_2$  (has a small feature at high temperature) and  $\text{Ru}_3(\text{CO})_{12}/\text{HDS-TiO}_2$  (has a much broader desorption feature starting at a lower temperature); even after the ligand removal, the differing cluster–surface interaction between the Ru and titania due to the passivated defects of the CVD sample changed the resultant available CO sites on the modified substrate.

### XPS results

**Ti 2p region – surface defects.** The Ti 2p regions were measured for  $\text{TiO}_2$  substrates and fitted using two sets of peak doublets, shown in Fig. 3a for NS-TiO<sub>2</sub> and Fig. 3b for HDS-TiO<sub>2</sub> as examples. The doublets correspond to the  $\text{Ti}^{4+}$  and  $\text{Ti}^{3+}$  oxidation states; for the  $2p_{3/2}$  state the former is found at 459.4 eV  $\pm$  0.2 eV, and the latter at 457.8 eV  $\pm$  0.2 eV. A higher Ar<sup>+</sup> sputter dose will yield more  $\text{Ti}^{3+}$ , which is related to titania defect states. The fitting of Ti 2p is complicated by a changing background signal between the lower and higher BE peaks of the Ti doublets, which led to a consistent discrepancy between the measured and the fitted spectra for all samples in the region between the peaks. To reduce the relative uncertainty, the fitting and analysis procedure was kept consistent for all Ti 2p measurements. The procedure for determining the errors for the XPS measurements are described in the ESI.† The results from the XPS fitting procedure are shown in Table 2.  $\text{Ti}^{\text{Total}}$  is the sum of both peak areas, and the ratio of  $\text{Ti}^{3+}/\text{Ti}^{\text{Total}}$  was used as an approximation for the concentration of surface defects for each substrate. As can be seen from Table 2, there is

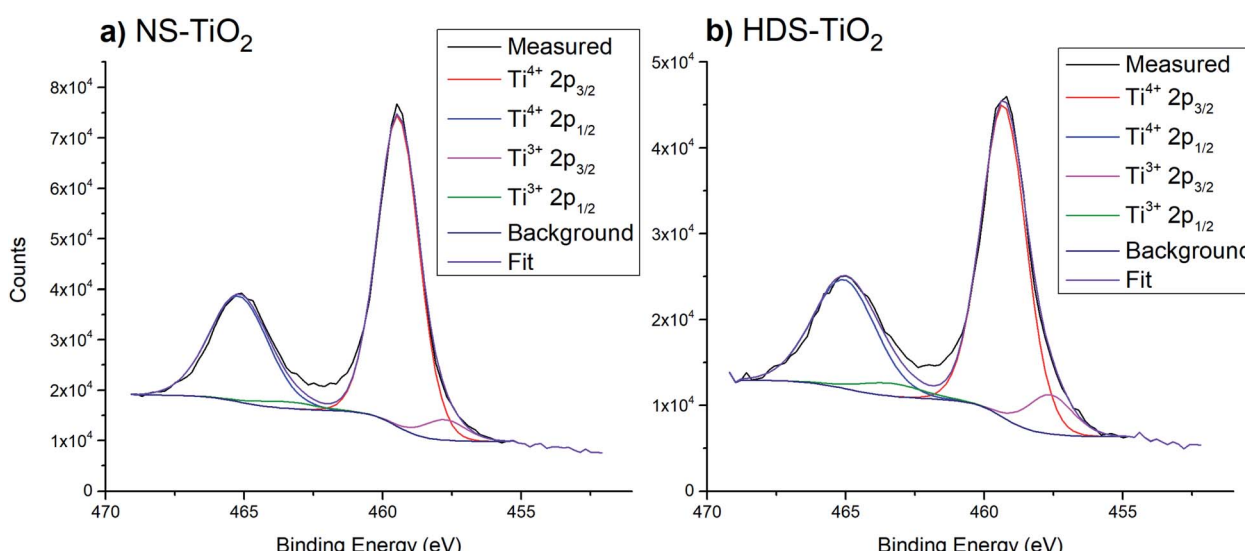


Fig. 3 Example peak fittings for Ti 2p region, after heating samples to 800 K. (a) NS-TiO<sub>2</sub>. (b) HDS-TiO<sub>2</sub>.



**Table 2** Summary of XPS atomic concentrations in % (at%) for  $\text{Ti}^{4+}$  and  $\text{Ti}^{3+}$  for blank and Ru cluster-loaded  $\text{TiO}_2$  samples. The  $\text{Ti}^{3+}/\text{Ti}^{\text{Total}}$  ratio in % was calculated according to  $\frac{100\% \times \text{at\%}(\text{Ti}^{3+})}{\text{at\%}(\text{Ti}^{\text{Total}})}$ . The uncertainty was  $\pm 1\%$  for  $\text{Ti}^{4+}$  at%, and  $\pm 15\%$  for both the  $\text{Ti}^{3+}$  at% and  $\text{Ti}^{3+}/\text{Ti}^{\text{Total}}$  ratio

Deposition	Substrate	Sample treatment	$\text{Ti}^{4+}$ at%	$\text{Ti}^{3+}$ at%	$\text{Ti}^{3+}/\text{Ti}^{\text{Total}}$ ratio (%)
Blank	NS- $\text{TiO}_2$	800 K heating	24.1	1.6	6
CS $\text{Ru}_3$	NS- $\text{TiO}_2$	As-deposited	22.2	0.8	3
CS $\text{Ru}_3$	NS- $\text{TiO}_2$	800 K heating	23.1	0.8	3
CS $\text{Ru}_3$	HDS- $\text{TiO}_2$	800 K heating	23.4	2.9	11
CVD $\text{Ru}_3(\text{CO})_{12}$	HDS- $\text{TiO}_2$	As-deposited ( <i>ex situ</i> )	16.9	0.3	2
CVD $\text{Ru}_3(\text{CO})_{12}$	HDS- $\text{TiO}_2$	800 K heating	23.2	1.0	4

a significantly higher defect density in the HDS- $\text{TiO}_2$  compared to NS- $\text{TiO}_2$ . The CVD samples were exposed to atmosphere and have a very low defect density. Further details are discussed in the ESI.<sup>†</sup>

**Ru 3d/C 1s region – clusters.** The main Ru 3d and C 1s peaks overlap in the same XPS region and were fitted together. No carbon was present in the stoichiometry of the substrate or clusters, excepting for ligated  $\text{Ru}_3(\text{CO})_{12}$ , and thus all carbon present was contamination on the surface or in the bulk structure of  $\text{TiO}_2$ . Three carbon peaks were used in the fitting, assigned to adventitious C-C at 285.0 eV; C-O ligands and contamination at 287.0 eV  $\pm 0.2$  eV; and COOH at 289.4 eV  $\pm 0.2$  eV. These are consistent to previously reported assignments for carbon contamination on  $\text{SiO}_2$  substrates.<sup>68</sup> The COOH peak was often completely removed upon heating. Fig. 4 shows an example of the peak fitting for the Ru 3d and C 1s region of a cluster-loaded sample, and Fig. 5 shows XPS results for Ru clusters on  $\text{SiO}_2$  and  $\text{TiO}_2$  after deposition of the  $\text{Ru}_3$  clusters and specific treatments. A summary of all Ru 3d/C 1s XPS measurements with BEs, at%, and Ru surface coverage is shown in Table 3. A Ru 3d spectrum of a metallic Ru reference sample is also shown in the ESI,<sup>†</sup> where the Ru 3d<sub>5/2</sub> peak is located at 279.7 eV  $\pm 0.2$  eV which is comparable to the BE reported by Morgan<sup>69</sup> for metallic Ru; 279.75 eV.

Based on the ratio of CO 1s at% to Ru 3d at%, the ratio of CO ligands to Ru atoms per cluster for the  $\text{Ru}_3(\text{CO})_{12}/\text{HDS-}\text{TiO}_2$  sample was calculated to be  $\sim 1.3$  after the cluster deposition (at% results for this are presented in the ESI<sup>†</sup>). This suggests an approximate average formula of  $\text{Ru}_3(\text{CO})_4$ , indicating some ligands are lost during the CVD process. However, the atomic ratio should be treated as an estimation because it may be affected by any adventitious carbon adsorbed during the CVD process. The number of CO ligands remaining after CVD depositions will be analysed in more detail in a subsequent publication.

The surface coverage was greater for  $\text{Ru}_3(\text{CO})_{12}/\text{HDS-}\text{TiO}_2$  than for all CS-deposited samples; for example, it is  $\sim 3$  times greater than  $\text{Ru}_3/\text{HDS-}\text{TiO}_2$ . However, all samples had only a fraction of a monolayer (ML) coverage (10.7% ML maximum). Due to the low coverages, it was assumed any cluster–cluster interactions were negligible and the differences in cluster loading would not have significantly affected the properties of the clusters when making comparisons between samples.

For  $\text{Ru}_3/\text{SiO}_2$  the Ru 3d<sub>5/2</sub> BE was at 280.7 eV  $\pm 0.2$  eV, and there was no peak shifting due to heating to 800 K, indicating there was no detectable change in oxidation state (see Table 3). For as-deposited  $\text{Ru}_3/\text{NS-}\text{TiO}_2$ , the Ru 3d<sub>5/2</sub> peak is found at 280.3  $\pm 0.2$  eV, and after heating to 800 K it is found at 280.5  $\pm 0.2$  eV, thus shifting by  $+0.2$  eV  $\pm 0.1$  eV (Table 3). The increase in BE indicated the clusters had become more positively charged, and the BE moved further away from the value for metallic Ru 3d<sub>5/2</sub> which is 279.7 eV  $\pm 0.2$  eV. It should be noted that the relative error in peak position for the same sample before and after heating is smaller than the error for the absolute peak position. For  $\text{Ru}_3/\text{NS-}\text{TiO}_2$  the as-deposited Ru 3d<sub>5/2</sub> peak increases from 280.2 eV to 280.4 eV after dosing with CO, which indicates Ru–CO bonding is occurring (see Table 3). For  $\text{Ru}_3/\text{HDS-}\text{TiO}_2$  the Ru 3d BE was compared after heating to 800 K, and then dosing with CO ligands. No shift in Ru 3d<sub>5/2</sub> BE was detected which provides evidence Ru–CO binding sites were not available on this sample (see Table 3). If Ru–CO binding was occurring one would reasonably expect an increase in BE, as was the case for dosing CO onto  $\text{Ru}_3/\text{NS-}\text{TiO}_2$ . This is supported by the earlier CO-TPD results showing that there was no Ru–CO binding sites available for  $\text{Ru}_3/\text{HDS-}\text{TiO}_2$  (Fig. 1d). For  $\text{Ru}_3(\text{CO})_{12}/\text{HDS-}\text{TiO}_2$ , the Ru 3d peak shifted by  $-1.4$  eV  $\pm 0.1$  eV to a BE of 280.6 eV  $\pm 0.2$  eV after heating, due to the loss of CO ligands (see Table 3). When

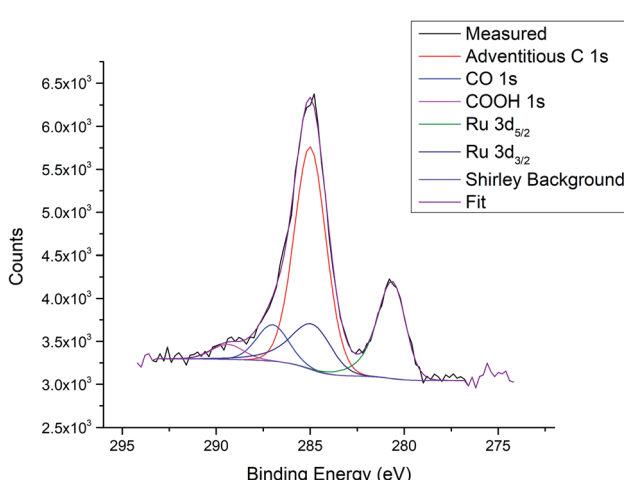


**Fig. 4** Example fitting for the Ru 3d/C 1s region; measurement of  $\text{Ru}_3/\text{HDS-}\text{TiO}_2$  after heating to 800 K.



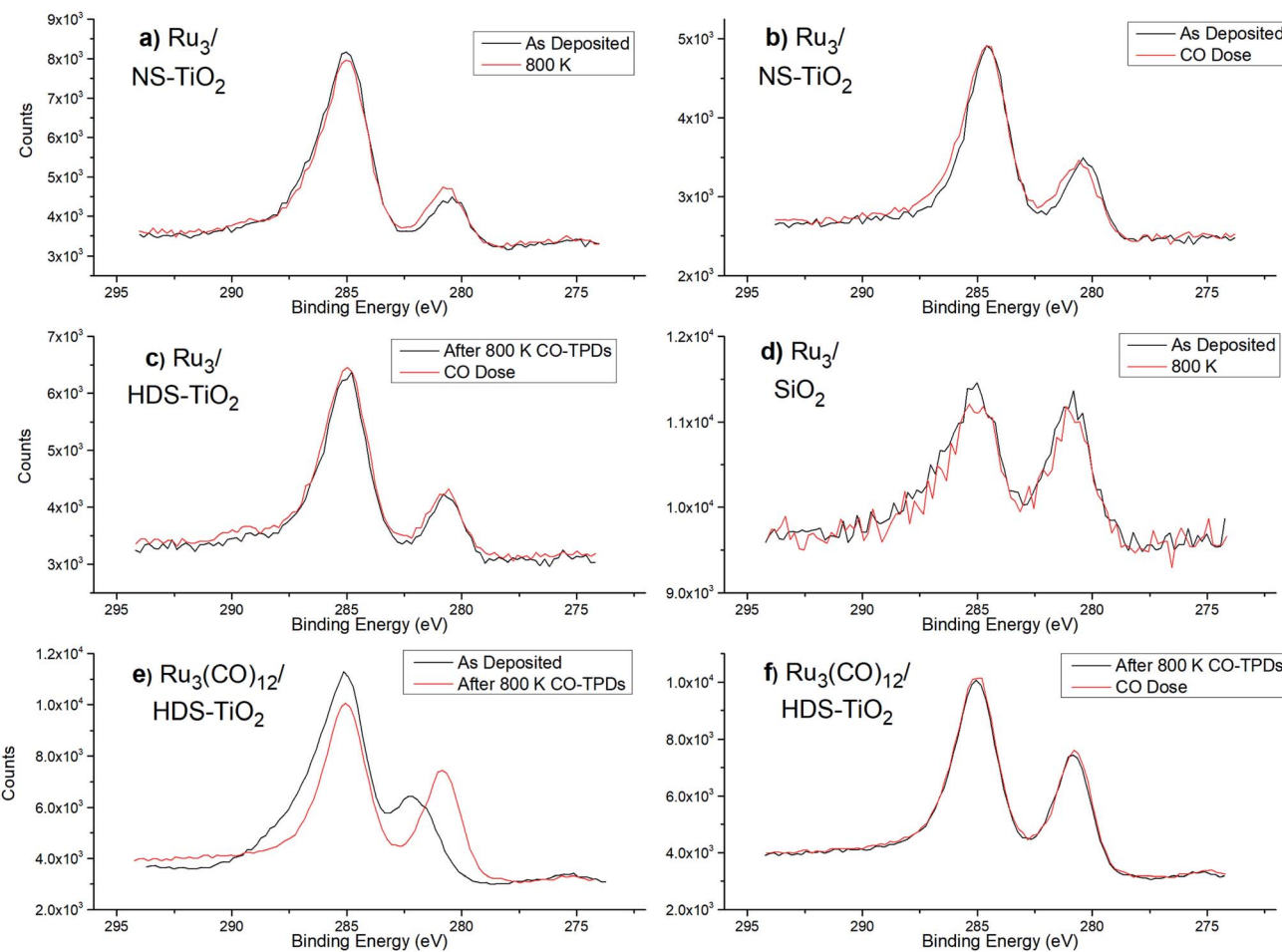


**Fig. 5** XPS spectra of Ru 3d/C 1s region for bare Ru<sub>3</sub> (a–d) and Ru<sub>3</sub>(CO)<sub>12</sub> (e–f) on different substrates. Different surface treatments are being compared with XPS, and some spectra are repetitive. The lower BE peaks at 280.2–282.0 eV are from Ru 3d<sub>5/2</sub> and are the peak of interest to determine peak shifting. (a) Ru<sub>3</sub>/NS-TiO<sub>2</sub> – as-deposited, and after heating to 800 K. (b) Ru<sub>3</sub>/NS-TiO<sub>2</sub> – as-deposited, and after CO dose. (c) Ru<sub>3</sub>/HDS-TiO<sub>2</sub> – after CO-TPD to 800 K, and after CO dose. (d) Ru<sub>3</sub>/SiO<sub>2</sub> – as-deposited, and after heating to 800 K. (e) Ru<sub>3</sub>(CO)<sub>12</sub>/HDS-TiO<sub>2</sub> – as-deposited, and after CO-TPD to 800 K. (f) Ru<sub>3</sub>(CO)<sub>12</sub>/HDS-TiO<sub>2</sub> – after CO-TPD to 800 K, and after CO dose (performed in series with the measurement in (e)).

dosing CO onto the clusters after the 800 K heating, there was no detectable shift in the Ru 3d BE (see Table 3), indicating after heating the Ru–CO sites are also blocked for Ru<sub>3</sub>(CO)<sub>12</sub>/HDS-

TiO<sub>2</sub>. This is supported by the earlier CO-TPD data which shows no characteristic Ru–CO desorption peaks for Ru<sub>3</sub>(CO)<sub>12</sub>/HDS-TiO<sub>2</sub> after the 1<sup>st</sup> CO-TPD cycle (Fig. 2).

**Table 3** Comparison of XPS results for different treatments of bare Ru<sub>3</sub> and Ru<sub>3</sub>(CO)<sub>12</sub> clusters on different substrates. Data is from peak fitting of the XPS spectra in Fig. 5. Ru 3d<sub>5/2</sub> BE, Ru at%, and Ru surface coverage are shown. Each row features XPS measurements before and after a sample treatment step, which have been separated into “Method 1” and “Method 2” (the method number only indicates the order of applying a treatment). Where none is shown for a method, this means the sample was as-deposited. Ru at% values are from method 1. For samples with an “800 K + CO Dose” method, the sample was cooled to 180 K before dosing. Both Ru<sub>3</sub>(CO)<sub>12</sub> measurements were performed on a single sample. The uncertainty in BEs was  $\pm 0.2$  eV, while for BE differences the uncertainty was  $\pm 0.1$  eV. Ru at% was  $\pm 4\%$ . The absolute error in the surface coverage was  $\sim 100\%$  while the relative uncertainty was based on the Ru at% and was  $\pm 4\%$

Deposition	Substrate	Ru at%	Surface coverage (% ML)	Method 1		Method 2		
				Method	BE (eV)	Method	BE (eV)	BE shift (eV)
CS Ru <sub>3</sub>	SiO <sub>2</sub>	0.55	4.0	None	280.7	800 K	280.7	0.0
CS Ru <sub>3</sub>	NS-TiO <sub>2</sub>	0.43	3.1	None	280.2	CO dose	280.4	0.2
CS Ru <sub>3</sub>	NS-TiO <sub>2</sub>	0.41	3.0	None	280.3	800 K	280.5	0.2
CS Ru <sub>3</sub>	HDS-TiO <sub>2</sub>	0.37	3.1	800 K	280.5	800 K + CO dose	280.5	0.0
CVD Ru <sub>3</sub> (CO) <sub>12</sub>	HDS-TiO <sub>2</sub>	1.48	10.7	None	282.0	800 K	280.6	-1.4
CVD Ru <sub>3</sub> (CO) <sub>12</sub>	HDS-TiO <sub>2</sub>	1.48	10.7	800 K	280.6	800 K + CO dose	280.6	0.0



## Discussion

As a brief summary of the results (*vide supra*), the adsorption of CO to CS-deposited  $\text{Ru}_3$  clusters was completely blocked when clusters were deposited onto LDS- $\text{TiO}_2$  or HDS- $\text{TiO}_2$ , but this was not the case for  $\text{SiO}_2$  or NS- $\text{TiO}_2$ . After  $\text{Ru}_3/\text{SiO}_2$  was heated to 800 K for a TPD cycle there was a decrease in temperature and size for the high temperature peak in the CO-TPD spectrum, while for  $\text{Ru}_3/\text{NS-TiO}_2$  heating caused the complete loss of the high temperature CO desorption peak. In XPS the Ru 3d BE for  $\text{Ru}_3/\text{NS-TiO}_2$  shifted to slightly higher energies after heating to 800 K, which is associated with a change in oxidation state of the clusters. The higher energy BE after heating to 800 K is shared in position by both  $\text{Ru}_3$  and  $\text{Ru}_3(\text{CO})_{12}$  on HDS- $\text{TiO}_2$ .

### Cluster agglomeration for $\text{Ru}_3/\text{SiO}_2$

For the  $\text{Ru}_3/\text{SiO}_2$  sample the decrease in temperature and size for the high temperature CO-TPD peak (Fig. 1a) was also associated with a decrease in total CO desorbing. This decrease cannot be explained by the clusters detaching or travelling into the substrate. First, once the clusters have adsorbed they are not likely to detach due to heating to 800 K because the bulk Ru boiling point is 4423 K.<sup>70</sup> Second, the clusters are unlikely to travel into the substrate because  $\text{SiO}_2$  is fairly inert and does not interact strongly with supported clusters<sup>30</sup> or typically form an SMSI with supported metals at these temperatures and conditions.<sup>67</sup> This decrease in CO desorption peak size is therefore attributed to cluster agglomeration. When clusters form larger aggregates the ratio of surface atoms to internal atoms for the clusters is reduced, thereby reducing the total number of CO binding sites on Ru clusters and agglomerated Ru clusters available in the system. A decrease in CO peak size due to cluster agglomeration has similarly been seen in other CO-TPD studies, such as studies by Anderson and co-workers on CS-deposited  $\text{Pt}_7/\text{alumina}$  and various sized  $\text{Pt}_n/\text{silica}$ ;<sup>71,72</sup> in these studies the CO-TPD spectra changed in shape with repeated TPD cycles to 700 K, where the higher temperature binding site similarly decreased in peak size and temperature. The agglomeration of Ru on  $\text{SiO}_2$  was not surprising and is most likely due to the weak cluster–surface interaction between Ru and  $\text{SiO}_2$ ; previous studies have also shown agglomeration of small clusters on  $\text{SiO}_2$  at temperatures below 800 K.<sup>63,73</sup>

In addition to aggregation of the Ru clusters, there is also most likely a change in either the cluster structure (beyond agglomeration) or cluster–surface interaction with repeated CO-TPD cycles; this is evidenced by the peak CO desorption temperature decreasing with each CO-TPD cycle, meaning CO is adsorbing less strongly to the clusters after agglomeration. This is also supported by earlier studies by Anderson and co-workers,<sup>59,71,72</sup> who have shown that for both  $\text{Pt}_n/\text{alumina}$  ( $2 \leq n \leq 18$ ) and  $\text{Pt}_n/\text{silica}$  ( $n = 4, 7, 12, 24$ ), the intensity of the high temperature CO-TPD peak increased as cluster size increased, but that repeated CO-TPD cycles caused the peak decrease in intensity and shift to lower temperatures. This provided evidence in the case of small Pt clusters that agglomeration

produces different structures than those produced by deposition of larger size-selected clusters.

By making reasonable assumptions, the increase in cluster size over the four CO-TPD cycles for  $\text{Ru}_3/\text{SiO}_2$  was estimated. The 4<sup>th</sup> cycle had 0.3 CO molecules desorbing per Ru atom compared to 0.6 CO per Ru atom in the 1<sup>st</sup> cycle (see Fig. 1a). Total CO desorption is proportional to the number of available CO binding sites. The simplest case to assume employs a model which disregards the individual atoms forming the clusters, instead considering hemispherical clusters pinned to the substrate where the number of binding sites is assumed to be proportional to the surface area (SA). If the bottom half of a hemispherical cluster is bound to the substrate and not available for binding to CO, then the available SA of the clusters would be given by eqn (1) for the surface area of a hemisphere.

$$\text{SA}_{\text{(hemisphere)}} = 2\pi r^2 \quad (1)$$

Utilising the number of CO desorbing per Ru atom in each cycle, and the assumption that available binding sites are proportional to the available SA, the increase in cluster radius is calculated as per eqn (2) and (3). Subscripts correspond to the SA or radius of clusters in the 1<sup>st</sup> or 4<sup>th</sup> cycle.

$$\frac{0.6 \text{ molecules per atom}}{0.3 \text{ molecules per atom}} = \frac{\text{SA}_{\text{(1st)}}}{\text{SA}_{\text{(4th)}}} \quad (2)$$

By substituting in the relationship between SA and radius for each cycle from eqn (1) and simplifying the expression, the change in radius can be estimated.

$$r_{\text{(4th)}} = 1.4 \times r_{\text{(1st)}} \quad (3)$$

The Ru cluster radius increases by an estimated factor of 1.4 after 4<sup>th</sup> CO-TPD cycles. Given that there would be a range of aggregated cluster sizes, this should be treated as an average size. The diameter of supported  $\text{Ru}_3$  is estimated to be 0.265 nm based on the interatomic Ru–Ru distance (bond length),<sup>74</sup> and the clusters therefore increase to an average diameter of 0.37 nm after the 4<sup>th</sup> CO-TPD cycle. The assumptions made in this calculation are rather simplified and must be taken with caution. The assumption of a hemispherical cluster is a rather simple model and likely deviates from the true structure of the supported clusters and also ignores the finite size of the atoms forming the clusters. The calculation also ignores any effects of the cluster structure and size, or the number of binding sites available per SA. For example, another possibility to describe the reduction in CO bond sites is a change from a  $\text{Ru}_3$  cluster adsorbed flat on the surface into a 3-dimensional  $\text{Ru}_6$  cluster (two  $\text{Ru}_3$  clusters on top of each other) that prevents the lower 3 Ru atoms from being exposed to incoming CO.

### Assigning binding sites to CO-TPD features

In the CO-TPD spectra, differences in temperatures for CO desorption could be due to the CO binding to chemically different parts of the cluster (*i.e.* a different binding site) or due to differing cluster–substrate interactions affecting the cluster–



CO binding. The shape of the CO desorption trace between successive CO-TPD cycles can provide information about the location of the Ru-CO binding sites on the clusters. This has been attempted in similar experiments including a study by Labich *et al.*<sup>75</sup> of Rh particles supported on  $\text{TiO}_2/\text{Mg}$  where an on-top position (away from the substrate, highest temperature) and two-fold coordinated bridge position (cluster–substrate bridging, medium temperature), as well as a third high-coverage state (low temperature) were identified. This study did not have sufficient TPD resolution to identify exact peak positions for the desorption features, but highlights the fact that when on a substrate, cluster–substrate  $\mu_2$  bridging bonds are also a possibility. This was also shown by Lee *et al.*<sup>76</sup> for  $\text{Au}_3$  clusters on  $\text{TiO}_2(110)$ , who argued that CO was bound to the cluster–substrate interface when dosed under UHV because the low energy ion scattering spectroscopy (LEIS) signal for Au was not attenuated by CO adsorption. Regarding the nature of Ru-CO bonds, White *et al.*<sup>77</sup> suggested *via* a DFT study that the optimised structure for  $\text{Ru}_3(\text{CO})_1$  features a 1.50 eV terminal  $\mu_1$  bond (CO bound to one Ru atom) while  $\text{Ru}_3(\text{CO})_2$  features an additional bridging  $\mu_2$  bond (CO bound to two Ru atoms) with a higher average Ru-CO bond energy of 1.79 eV. This calculation was performed in the gas phase and although not directly comparable to supported clusters it importantly indicates that  $\mu_1$  and  $\mu_2$  bonding are possible.

The peaks will first be assigned for the  $\text{Ru}_3/\text{SiO}_2$  sample, which is treated as the baseline for comparisons. As mentioned in the ESI,† the accuracy of the absolute TPD intensity calibration is estimated to be  $\sim 50\%$ . Fig. 1a shows that in the 1<sup>st</sup> cycle there was an average of 0.6 CO adsorbed per Ru atom, or 1.7 CO per  $\text{Ru}_3$  cluster. Given the  $\sim 50\%$  estimated accuracy, it is likely that most clusters had 2 CO per cluster after dosing. The clusters were agglomerated on  $\text{SiO}_2$  with each successive CO-TPD cycle, and the main 560 K CO desorption site decreased in size successively while the smaller 260 K desorption feature increased in size after one cycle and then stabilized. As the clusters agglomerate, the total number of CO “edge sites” available where the cluster meets the substrate is expected to decrease. Understanding this helps to assign the two main features in Fig. 1a. The 560 K peak is most likely from a  $\mu_2$  cluster–substrate bridging site on the cluster edges; this is supported because the CO-TPD peak size decreases, due to a decrease in the number of edge sites that would occur on agglomeration (as discussed above), and because the higher binding energy of the site supports the likelihood of CO bonding to both the cluster and substrate. This peak also decreases in temperature, which provides evidence that the adsorption energy of CO to the cluster–substrate bridging sites decreases as clusters agglomerate, which would be related to a change in cluster charge density. The 260 K feature is most likely from an on-top binding site with  $\mu_1$  and/or  $\mu_2$  Ru–Ru bonding. The increase in the 260 K peak size after the 1<sup>st</sup> cycle may indicate that some amount of agglomeration promoted the number of on-top sites compared to edge sites. Regarding the CO-TPD samples on  $\text{TiO}_2$  substrates, for  $\text{Ru}_3/\text{NS-TiO}_2$  the CO-TPD spectrum (Fig. 1b) is very similar to  $\text{Ru}_3/\text{SiO}_2$  in the 1<sup>st</sup> cycle. The assignment of peaks is therefore the same as for  $\text{Ru}_3/$

$\text{SiO}_2$  but with the peaks shifted in temperature. For bare  $\text{Ru}_3$  on sputtered  $\text{TiO}_2$  surfaces (Fig. 1c and d), no Ru-CO peaks are observed and there are no CO binding sites to assign.

For the ligated sample,  $\text{Ru}_3(\text{CO})_{12}/\text{HDS-TiO}_2$ , the high temperature peak in the 1<sup>st</sup> cycle at 600 K appears to be a shifted version of the same feature as the high temperature peak for  $\text{Ru}_3/\text{NS-TiO}_2$ , and is assigned to cluster–substrate bridging sites. As previously discussed, this peak is wider in temperature than for the large desorption peak of either  $\text{Ru}_3/\text{NS-TiO}_2$  or  $\text{Ru}_3/\text{SiO}_2$ , which may indicate a wider range of binding energies for bridging sites in this sample, possibly as a result of the larger number of CO molecules per Ru atom. The peak at 300 K (Fig. 2) is assigned to on-top CO with  $\mu_1$  and/or  $\mu_2$  bonding, the same as for the other samples. The 1<sup>st</sup> cycle CO-TPD spectrum of  $\text{Ru}_3(\text{CO})_{12}/\text{HDS-TiO}_2$  (Fig. 2) is similar to what Zhao *et al.*<sup>19</sup> previously measured for  $\text{Ru}_3(\text{CO})_{12}$  on  $\text{TiO}_2(110)$  when deposited by CVD at 300 K. However, a key difference is the peaks for Zhao *et al.* were higher at  $\sim 400$  K and  $\sim 650$  K, and the higher peak had an extra low-temperature shoulder not seen in Fig. 2. It is likely these differences are related to differences in cluster–surface interaction between the  $\text{TiO}_2(110)$  used in that study and HDS-TiO<sub>2</sub> used in this study. Zhao *et al.*<sup>19</sup> did not assign binding sites to the CO-TPD spectra, however they interestingly discovered that the large, broad high temperature CO desorption feature was not present when  $\text{Ru}_3(\text{CO})_{12}$  clusters were deposited by CVD onto a substrate at 100 K (instead of 300 K); the spectra instead had 5 smaller, narrow features.<sup>19</sup> This further supports the notion that the high temperature peak is related to cluster–substrate bridging, because this kind of binding would most likely be promoted when depositing onto a higher temperature substrate which can more easily interact with the clusters.

## Oxidation of Ru clusters

The Ru 3d BE for  $\text{Ru}_3/\text{NS-TiO}_2$  shifted higher to 280.5 eV  $\pm$  0.2 eV after heating (Table 3), and is comparable to studies in the literature<sup>18,19</sup> where  $\text{O}_2$  was dosed onto  $\text{Ru}_3(\text{CO})_{12}$  on  $\text{TiO}_2(110)$  with heating to intentionally form oxidised clusters. In these cases, similar BE shifts were measured and absolute values for Ru 3d<sub>5/2</sub> were reported as 280.6 eV by Zhao *et al.*<sup>19</sup> and 280.8 eV by Rizzi *et al.*<sup>18</sup> The similarity between these and the present study provides context for the previously discussed loss of the main 560 K CO desorption peak for  $\text{Ru}_3/\text{NS-TiO}_2$  after heating to 800 K (Fig. 1b). The XPS peak shifting and CO-TPD results both point towards the oxidation of the Ru clusters, presumably due to an interaction with the oxygen in the supporting  $\text{TiO}_2$  ( $\text{O}_2$  was not dosed onto the clusters). The blocked CO-TPD peak is assigned to cluster–substrate bridging sites, and thus oxygen is either binding to these sites or sterically hindering the access of CO to the sites. The shifted Ru 3d<sub>5/2</sub> XPS peak is thus assigned to a partially oxidised form of the clusters. The increase in oxidation state can also be a reason for making Ru less attractive for binding to CO ligands. It should be noted that bulk Ru shows a BE shift of 1.6 eV upon oxidation<sup>69</sup> and that the BEs reported in the literature for oxidised Ru clusters are lower than those typically reported for oxidised bulk



Ru such as  $\text{RuO}_2$ .<sup>69</sup> Thus, it is difficult to determine the exact oxidation state for Ru clusters on  $\text{Ru}_3/\text{NS-TiO}_2$ .

As-deposited XPS was not measured for  $\text{Ru}_3/\text{HDS-TiO}_2$  but at 800 K. However the BE for Ru  $3\text{d}_{5/2}$  at 800 K was 280.5 eV  $\pm$  0.2 eV, identical to that of  $\text{Ru}_3/\text{NS-TiO}_2$  (Table 3). Thus, the clusters are most likely oxidised by the  $\text{TiO}_2$  surface upon heating to 800 K on HDS-TiO<sub>2</sub> in the same way as NS-TiO<sub>2</sub>. The BE for  $\text{Ru}_3(\text{CO})_{12}/\text{HDS-RF-TiO}_2$  after heating to 800 K is also the same as both  $\text{Ru}_3/\text{NS-TiO}_2$  and  $\text{Ru}_3/\text{HDS-TiO}_2$  within the experimental uncertainty, indicating that the initially-ligated clusters are also partially oxidised by the  $\text{TiO}_2$  substrate once their ligands had been removed by heating. The CO-TPD results for  $\text{Ru}_3/\text{SiO}_2$  do not indicate any change in oxidation state of the clusters due to heating. It is also worth noting that in the case of Ru the cluster size does not seem to influence the BE, and thus the agglomeration discussed above on  $\text{SiO}_2$  did not result in a change in BE, which is different to other metals like gold.<sup>31,78-83</sup> The lack of change in Ru oxidation state on  $\text{SiO}_2$  is most likely due to the fact that it is a non-reducible oxide, while  $\text{TiO}_2$  is a reducible oxide.<sup>65</sup> The removal of  $\text{O}^{2-}$  from non-reducible oxides such as  $\text{SiO}_2$  is energetically unfavourable and these oxides are more stoichiometrically stable and less reactive.<sup>65,66</sup> Evidence of the substrate-dependent oxidation of clusters has been shown in other studies, and oxidation is typical of the SMSI for clusters on metal-oxide supports.<sup>33,84,85</sup>

It is likely that the mechanism of cluster oxidation on  $\text{TiO}_2$  is related to the minimisation of surface energy, where there is an energetic benefit for the system from the oxidation of Ru. The surface free energy of Ru at 298 K has been determined experimentally to be  $3.409 \text{ J m}^{-2}$ ,<sup>86</sup> while the surface free energy of  $\text{RuO}_2$  was calculated in a separate DFT study as  $1.1 \text{ J m}^{-2}$  for  $\text{RuO}_2(110)$  and  $1.4 \text{ J m}^{-2}$  for  $\text{RuO}_2(100)$ .<sup>87</sup> These two studies used different calculation methods and are not quantitatively comparable for determining the precise change in surface free energy, however the lower surface free energy of  $\text{RuO}_2$  than Ru provides evidence for the surface-energy minimisation benefit of Ru oxidation. The reduction of surface free energy due to oxidation has been shown more explicitly using calculations for other transition metals.<sup>88</sup> This mechanism can also be considered in terms of the negative enthalpy of formation for oxidised Ru; the energy of formation of transition metal oxides is typically negative, meaning there is an energetic benefit for oxidation and the clusters would lose energy to their surroundings when an oxide is formed.<sup>89,90</sup> Both the surface energy and the enthalpy considerations have the same meaning.

Heating is required for Ru cluster oxidation on NS-TiO<sub>2</sub>. The as-deposited  $\text{Ru}_3$  clusters on NS-TiO<sub>2</sub> showed the lowest oxidation state based on the XPS results, but the oxidation state increased upon heating to 800 K, even after the temperature was reduced. It is probable that for oxidation the transport of  $\text{O}^{2-}$  anions on the substrate must be activated by heating such that they are mobilized and can be transported to the clusters; the idea of bulk  $\text{TiO}_2$  defects becoming mobile at elevated temperatures and interacting with supported metals has been suggested previously.<sup>30,33,91</sup>

Zhao *et al.*<sup>19</sup> have previously deposited  $\text{Ru}_3(\text{CO})_{12}$  by CVD onto  $\text{TiO}_2(110)$ . After heating and ligand removal the authors

found that the Ru  $3\text{d}_{5/2}$  peak was located at 279.9 eV, which is comparable to bulk Ru. They found by dosing 400 L  $\text{O}_2$  under UHV at 600 K that the Ru peaks shifted higher to 280.6 eV, which they associated with oxidation of the clusters. The necessity for dosing  $\text{O}_2$  contrasts with our results on NS-TiO<sub>2</sub> where the clusters were oxidised after only heating to 800 K under UHV. This serves to demonstrate the fact that the SMSI interaction depends greatly on the combination of cluster and substrate, even including different forms of the same material such as  $\text{TiO}_2(100)$  in the work of Zhao *et al.*<sup>19</sup> and RF-deposited  $\text{TiO}_2$  in this study. Zhao *et al.* estimated that the cluster coverage was 5% to 25% of a monolayer, which is comparable to this study, so surface coverage cannot be the reason for the difference in results.<sup>19</sup> It is most likely that the different outcome is related to the differences between RF-deposited  $\text{TiO}_2$  and single crystal  $\text{TiO}_2(110)$  substrates; it is possible that  $\text{TiO}_2(110)$  is not as easily reducible, or that the surface energy is lower meaning there is less of a driving force for cluster oxidation in terms of surface energy minimization.

### Complete blocking of Ru-CO binding sites

The blocking or changing of some Ru-CO sites seen in the CO-TPD data have been above attributed to both agglomeration and oxidation. However, for  $\text{Ru}_3$  on LDS-TiO<sub>2</sub> and HDS-TiO<sub>2</sub> all Ru-CO binding sites are completely blocked such that no CO is able to adsorb to the clusters when dosed under UHV. The Ru-CO blocking cannot be associated with agglomeration only as this would result in CO-TPD spectra like that of  $\text{Ru}_3/\text{SiO}_2$  (Fig. 1a), or oxidation only as this would result in CO-TPD spectra like that of  $\text{Ru}_3/\text{NS-TiO}_2$  (Fig. 1b). For  $\text{Ru}_3(\text{CO})_{12}/\text{HDS-TiO}_2$ , the Ru-CO sites were present in the 1<sup>st</sup> CO-TPD cycle (before the ligands were desorbed) but were completely blocked in the 2<sup>nd</sup> and 3<sup>rd</sup> cycles after heating to 800 K. This result also contrasts the previously mentioned study by Zhao *et al.*<sup>19</sup> where XPS peak shifting was used to show Ru-CO binding was not blocked for  $\text{Ru}_3(\text{CO})_{12}$  on non-sputtered  $\text{TiO}_2(110)$  even when heated to 700 K.

For cases where Ru-CO sites are completely blocked there seems to be another reason for the complete loss of Ru-CO sites besides agglomeration or oxidation. The fact that Ru-CO sites were only completely blocked if RF-TiO<sub>2</sub> was sputter treated, in addition to the differences between depositions onto RF-deposited  $\text{TiO}_2$  in this study and  $\text{TiO}_2(110)$  in other studies,<sup>19</sup> raises a question about the mechanism of site-blocking. Encapsulation is another phenomenon which can occur for metals supported on a reducible oxide like  $\text{TiO}_2$ . This involves the mass transport of substrate material to the top of the clusters, effectively covering them. This has been shown in the literature for several types of clusters on  $\text{TiO}_2$  substrates, including the study by Fu *et al.*<sup>33</sup> of 1.5 nm Pd clusters grown on  $\text{TiO}_2(110)$  as well as many other examples over the past few decades.<sup>32,34,55,75,92-96</sup> Encapsulation is related to the formation of an SMSI state, and there are various proposed reaction mechanisms for encapsulation in the literature, including thermodynamic drive to minimize the total surface energy of the system.<sup>33,75,92,93,96,97</sup> This mechanism is most likely to occur when



the surface energy of the metal is greater than the surface energy of the supporting oxide layer,<sup>33,75,93,97</sup> which is the case for Ru and TiO<sub>2</sub>; as indicated above, the surface energy of Ru is 3.409 J m<sup>-2</sup> and TiO<sub>2</sub>(110) has been calculated to be 1.78 J m<sup>-2</sup>.<sup>64,98</sup>

Given the propensity of TiO<sub>2</sub> to encapsulate surface adsorbates, it is possible that the complete loss of Ru-CO binding sites for Ru<sub>3</sub>(CO)<sub>12</sub>/HDS-TiO<sub>2</sub> is due to cluster encapsulation by the substrate material, possibly in combination with other phenomena such as oxidation and/or agglomeration. However, the occurrence of encapsulation is not entirely clear because the data does not directly show the encapsulation, only the indirect blocking of Ru-CO sites. From previous literature, varying conditions have been reported to induce cluster encapsulation which typically require high temperature reduction of the oxide substrate under UHV<sup>32-34,64,75,92-96,99,100</sup> or H<sub>2</sub>.<sup>101-105</sup> A notable similarity of the results here to encapsulation occurring in previous studies for Pd and Rh clusters on TiO<sub>2</sub>(110) is that sputtering of the substrate prior to cluster deposition was shown to be required for encapsulation.<sup>33,34</sup> In the present study, Ru-CO binding sites were only completely blocked for Ru<sub>3</sub> on sputtered TiO<sub>2</sub>, providing evidence that surface roughness and/or oxygen deficiency play a role in the state of Ru clusters on the surface. However, a key difference is that in the current study Ru-CO blocking occurs in as-deposited Ru<sub>3</sub>/HDS-TiO<sub>2</sub> with no heating required.<sup>33,34</sup> Thus, this may point towards a different site-blocking mechanism which is unique for the RF-deposited TiO<sub>2</sub> substrate. Other causes for the site blocking may be sub-surface defects caused by sputter treatment<sup>34</sup> which attract the clusters below the surface, or subsurface oxygen being more readily available for the Ru<sub>3</sub> than surface oxygen and the subsurface oxygen similarly attracting the clusters. To the best of our knowledge there have been no previous measurements for the encapsulation of size-selected Ru clusters on TiO<sub>2</sub> in the literature, although some encapsulation studies using similar Ru materials have been conducted.<sup>55,106</sup> Further insight into the mechanisms of interactions of Ru clusters with TiO<sub>2</sub> will be shown in a subsequent publication. It should be noted that the present work does not allow determining the change of the Ru cluster size due to the heating procedures applied. This will be subject to a subsequent publication.

The blocking of cluster-CO binding sites is not generally desired for catalytic purposes because CO adsorption capacity is reduced, which is the case for some samples in this study as well as other reports in the literature.<sup>33,34,75</sup> As such the results discussed can provide a framework for how to achieve Ru clusters on TiO<sub>2</sub> supports with available Ru-CO binding sites for the catalysis of reactions such as CO hydrogenation. While it is possible that conserving Ru-CO binding sites is important for catalytic activity, there have been cases which showed that if a covering layer is thin enough some combinations of cluster and covering layer can have an electronic structure which is suitable for catalysis without direct reactant-cluster contact.<sup>107-109</sup> In these cases, there can be extra benefits for catalysis such as increasing resistance to cluster agglomeration,<sup>107,108</sup> increasing catalytic reaction selectivity,<sup>109</sup> or improving catalytic activity by hindering back reactions which

remove reaction products.<sup>108</sup> As such, catalysis measurements are necessary for experimental verification of this framework.

## Conclusions

For Ru<sub>3</sub> CS-deposited onto SiO<sub>2</sub>, heating the clusters to 800 K caused cluster agglomeration. Conversely, for Ru<sub>3</sub> CS-deposited onto NS-TiO<sub>2</sub>, the clusters remained on the surface but were oxidised by the substrate when heated to 800 K, resulting in the loss of the main CO binding site. This indicated oxygen either bound to the same sites as CO or bound in such a way that CO was sterically hindered, or Ru was less attractive for binding to CO due to an increase in oxidation state. When the TiO<sub>2</sub> substrate was Ar<sup>+</sup> sputter treated before CS-depositions the Ru-CO binding sites on the clusters were completely blocked by the substrate as-deposited. For Ru<sub>3</sub>(CO)<sub>12</sub>/HDS-TiO<sub>2</sub>, the clusters retained their Ru-CO sites as-deposited but after heating to 800 K the ligands were removed, and the Ru-CO sites were completely blocked. It is possible given the lack of Ru-CO binding sites that the catalytic abilities of the small Ru clusters will be reduced when supported on sputtered TiO<sub>2</sub>.

We have developed a set of deposition criteria for Ru<sub>3</sub> clusters to retain their Ru-CO binding sites when supported on RF-deposited TiO<sub>2</sub>. For CS depositions the Ru-CO sites will be blocked if the substrate is sputter treated prior to deposition, but when depositing Ru<sub>3</sub>(CO)<sub>12</sub> by CVD the CO ligands are retained on a sputtered substrate. In both cases heating to 800 K will cause cluster oxidation (a partial loss of CO sites) and/or complete Ru-CO blocking. The mechanism for complete Ru-CO blocking on sputtered TiO<sub>2</sub> could not be precisely determined from the presented results, but comparisons to similar studies of metal/TiO<sub>2</sub>(100) interfaces point towards an interpretation that the clusters were encapsulated by a layer of substrate material. A key difference to previous studies was that no heating was required for Ru-CO blocking to occur, possibly pointing to a unique mechanism for site blocking by RF-deposited TiO<sub>2</sub>.

## Conflicts of interest

There are no conflicts to declare.

## Acknowledgements

The work is supported by the US army project FA5209-16-R-0017. Part of the work is supported by the Australian Solar Thermal Research Institute (ASTRI), a project supported by the Australian Government, through the Australian Renewable Energy Agency (ARENA). The work at the University of Utah was partly supported by the Air Force Office of Scientific Research, under AFOSR grant FA9550-19-1-0261. The authors acknowledge the facilities, and the scientific and technical assistance, of Microscopy Australia (formerly known as AMMRF) and the Australian National Fabrication Facility (ANFF) at Flinders University. The authors acknowledge Flinders Microscopy and Microanalysis and their expertise.



## References

1 D. Lee, R. L. Donkers, G. Wang, A. S. Harper and R. W. Murray, Electrochemistry and optical absorbance and luminescence of molecule-like Au<sub>38</sub> nanoparticles, *J. Am. Chem. Soc.*, 2004, **126**, 6193–6199.

2 J. Jung, H. Kim and Y.-K. Han, Can an electron-shell closing model explain the structure and stability of ligand-stabilized metal clusters?, *J. Am. Chem. Soc.*, 2011, **133**, 6090–6095.

3 G. Ramakrishna, O. Varnavski, J. Kim, D. Lee and T. Goodson, Quantum-sized gold clusters as efficient two-photon absorbers, *J. Am. Chem. Soc.*, 2008, **130**, 5032–5033.

4 M. Valden, X. Lai and D. W. Goodman, Onset of catalytic activity of gold clusters on titania with the appearance of nonmetallic properties, *Science*, 1998, **281**, 1647–1650.

5 C. Xu, X. Lai, G. Zajac and D. Goodman, Scanning tunneling microscopy studies of the TiO<sub>2</sub> (110) surface: structure and the nucleation growth of Pd, *Phys. Rev. B: Condens. Matter Mater. Phys.*, 1997, **56**, 13464.

6 C. P. Joshi, M. S. Bootharaju and O. M. Bakr, Tuning properties in silver clusters, *J. Phys. Chem. Lett.*, 2015, **6**, 3023–3035.

7 A. Sanchez, S. Abbet, U. Heiz, W. D. Schneider, H. Hakkinen, R. N. Barnett and U. Landman, When gold is not noble: nanoscale gold catalysts, *J. Phys. Chem. A*, 1999, **103**, 9573.

8 C. Moreno-Castilla, M. A. Salas-Peregrín and F. J. López-Garzón, Hydrogenation of carbon oxides by Ru/activated carbon catalysts obtained from Ru<sub>3</sub>(CO)<sub>12</sub>: effect of pretreatment on their dispersion, composition and activity, *J. Mol. Catal. A: Chem.*, 1995, **95**, 223–233.

9 P. Panagiotopoulou, Hydrogenation of CO<sub>2</sub> over supported noble metal catalysts, *Appl. Catal., A*, 2017, **542**, 63–70.

10 R. Mutschler, E. Moioli and A. Züttel, Modelling the CO<sub>2</sub> hydrogenation reaction over Co, Ni and Ru/Al<sub>2</sub>O<sub>3</sub>, *J. Catal.*, 2019, **375**, 193–201.

11 G. D. Weatherbee and C. H. Bartholomew, Hydrogenation of CO<sub>2</sub> on group VIII metals: IV. Specific activities and selectivities of silica-supported Co, Fe, and Ru, *J. Catal.*, 1984, **87**, 352–362.

12 K. Asakura and Y. Iwasawa, Surface structure and catalysis for CO hydrogenation of the supported Ru species derived from the Ru<sub>3</sub>(CO)<sub>12</sub> inorganic oxides, *J. Chem. Soc., Faraday Trans.*, 1990, **86**, 2657–2662.

13 F. Solymosi, A. Erdöhelyi and M. Kocsis, Methanation of CO<sub>2</sub> on supported Ru catalysts, *J. Chem. Soc., Faraday Trans.*, 1981, **77**, 1003–1012.

14 W. R. Hastings, C. J. Cameron, M. J. Thomas and M. C. Baird, Carbon monoxide and carbon dioxide hydrogenation catalyzed by supported ruthenium carbonyl clusters. A novel procedure for encapsulating triruthenium dodecacarbonyl within the pores of Na-Y zeolite, *Inorg. Chem.*, 1988, **27**, 3024–3028.

15 C. S. Kellner and A. T. Bell, Effects of dispersion on the activity and selectivity of alumina-supported ruthenium catalysts for carbon monoxide hydrogenation, *J. Catal.*, 1982, **75**, 251–261.

16 R. D. Gonzalez and H. Miura, Methanation and Fischer-Tropsch studies on potassium-promoted silica-supported Ru catalysts, *J. Catal.*, 1982, **77**, 338–347.

17 E. Kikuchi, H. Nomura, M. Matsumoto and Y. Morita, Fischer-tropsch synthesis of hydrocarbons on V<sub>2</sub>O<sub>3</sub>-supported ruthenium catalysts, *Appl. Catal.*, 1983, **7**, 1–9.

18 G. A. Rizzi, A. Magrin and G. Granozzi, Substitutional Ti(1-x)Ru<sub>x</sub>O<sub>2</sub> surface alloys obtained from the decomposition of Ru<sub>3</sub>(CO)<sub>12</sub> on TiO<sub>2</sub> (110), *Phys. Chem. Chem. Phys.*, 1999, **1**, 709–711.

19 X. Zhao, J. Hrbek and J. A. Rodriguez, The decomposition and chemistry of Ru<sub>3</sub>(CO)<sub>12</sub> on TiO<sub>2</sub> (110) studied with X-ray photoelectron spectroscopy and temperature programmed desorption, *Surf. Sci.*, 2005, **575**, 115–124.

20 D. Meier, G. Rizzi, G. Granozzi, X. Lai and D. Goodman, Ru<sub>3</sub>(CO)<sub>12</sub> adsorption and decomposition on TiO<sub>2</sub>, *Langmuir*, 2002, **18**, 698–705.

21 T. Cai, Z. Song, Z. Chang, G. Liu, J. Rodriguez and J. Hrbek, Ru nanoclusters prepared by Ru<sub>3</sub>(CO)<sub>12</sub> deposition on Au (111), *Surf. Sci.*, 2003, **538**, 76–88.

22 F. Yang, S. Kundu, A. B. Vidal, J. Graciani, P. J. Ramírez, S. D. Senanayake, D. Stacchiola, J. Evans, P. Liu and J. F. Sanz, Determining the Behavior of RuO<sub>x</sub> Nanoparticles in Mixed-Metal Oxides: Structural and Catalytic Properties of RuO<sub>2</sub>/TiO<sub>2</sub> (110) Surfaces, *Angew. Chem., Int. Ed.*, 2011, **50**, 10198–10202.

23 K. Asakura, K.-K. Bando and Y. Iwasawa, Structure and behaviour of Ru<sub>3</sub>(CO)<sub>12</sub> supported on inorganic oxide surfaces, studied by EXAFS, infrared spectroscopy and temperature-programmed decomposition, *J. Chem. Soc., Faraday Trans.*, 1990, **86**, 2645–2655.

24 P. Serp, P. Kalck and R. Feurer, Chemical vapor deposition methods for the controlled preparation of supported catalytic materials, *Chem. Rev.*, 2002, **102**, 3085–3128.

25 J. A. Rodriguez, J. Dvorak, T. Jirsak and J. Hrbek, Formation of Mo and MoS<sub>x</sub> nanoparticles on Au (111) from Mo(CO)<sub>6</sub> and S<sub>2</sub> precursors: electronic and chemical properties, *Surf. Sci.*, 2001, **490**, 315–326.

26 R. Psaro and S. Recchia, Supported metals derived from organometallics, *Catal. Today*, 1998, **41**, 139–147.

27 M. Xu and F. Zaera, Mechanistic studies of the thermal decomposition of metal carbonyls on Ni (100) surfaces in connection with chemical vapor deposition processes, *J. Vac. Sci. Technol., A*, 1996, **14**, 415–424.

28 A. C. Papageorgiou, K. Diller, S. Fischer, F. Allegretti, F. Klappenberger, S. C. Oh, O. z. Sağlam, J. Reichert, A. Wiengarten and K. Seufert, In Vacuo Porphyrin Metalation on Ag(111) via Chemical Vapor Deposition of Ru<sub>3</sub>(CO)<sub>12</sub>: Mechanistic Insights, *J. Phys. Chem. C*, 2016, **120**, 8751–8758.

29 E. Mohimi, Z. V. Zhang, S. Liu, J. L. Mallek, G. S. Girolami and J. R. Abelson, Area selective CVD of metallic films from molybdenum, iron, and ruthenium carbonyl precursors: Use of ammonia to inhibit nucleation on oxide surfaces, *J. Vac. Sci. Technol., A*, 2018, **36**, 041507.



30 U. Diebold, The surface science of titanium dioxide, *Surf. Sci. Rep.*, 2003, **48**, 53–229.

31 H. S. Al Qahtani, K. Kimoto, T. Bennett, J. F. Alvino, G. G. Andersson, G. F. Metha, V. B. Golovko, T. Sasaki and T. Nakayama, Atomically resolved structure of ligand-protected Au<sub>9</sub> clusters on TiO<sub>2</sub> nanosheets using aberration-corrected STEM, *J. Chem. Phys.*, 2016, **144**, 114703.

32 R. Bennett, C. Pang, N. Perkins, R. Smith, P. Morrall, R. Kwon and M. Bowker, Surface structures in the SMSI state; Pd on (1×2) reconstructed TiO<sub>2</sub> (110), *J. Phys. Chem. B*, 2002, **106**, 4688–4696.

33 Q. Fu, T. Wagner, S. Olliges and H.-D. Carstanjen, Metal-oxide interfacial reactions: Encapsulation of Pd on TiO<sub>2</sub> (110), *J. Phys. Chem. B*, 2005, **109**, 944–951.

34 A. Berkó, I. Ulrych and K. Prince, Encapsulation of Rh nanoparticles supported on TiO<sub>2</sub> (110)-(1×1) surface: XPS and STM studies, *J. Phys. Chem. B*, 1998, **102**, 3379–3386.

35 F. X. Xiao, S. F. Hung, J. Miao, H. Y. Wang, H. Yang and B. Liu, Metal-Cluster-Decorated TiO<sub>2</sub> Nanotube Arrays: A Composite Heterostructure toward Versatile Photocatalytic and Photoelectrochemical Applications, *Small*, 2015, **11**, 554–567.

36 I. X. Green, W. Tang, M. Neurock and J. T. Yates, Spectroscopic observation of dual catalytic sites during oxidation of CO on a Au/TiO<sub>2</sub> catalyst, *Science*, 2011, **333**, 736–739.

37 A. C. Reber, S. N. Khanna, F. S. Roberts and S. L. Anderson, Effect of O<sub>2</sub> and CO Exposure on the Photoelectron Spectroscopy of Size-Selected Pd n Clusters Supported on TiO<sub>2</sub> (110), *J. Phys. Chem. C*, 2016, **120**, 2126–2138.

38 H. S. Al Qahtani, G. F. Metha, R. B. Walsh, V. B. Golovko, G. G. Andersson and T. Nakayama, Aggregation behavior of ligand-protected Au<sub>9</sub> clusters on sputtered atomic layer deposition TiO<sub>2</sub>, *J. Phys. Chem. C*, 2017, **121**, 10781–10789.

39 F. S. Roberts, S. L. Anderson, A. C. Reber and S. N. Khanna, Initial and Final State Effects in the Ultraviolet and X-ray Photoelectron Spectroscopy (UPS and XPS) of Size-Selected Pd n Clusters Supported on TiO<sub>2</sub> (110), *J. Phys. Chem. C*, 2015, **119**, 6033–6046.

40 J.-Y. Ruzicka, F. Abu Bakar, C. Hoeck, R. Adnan, C. McNicoll, T. Kemmitt, B. C. Cowie, G. F. Metha, G. G. Andersson and V. B. Golovko, Toward Control of Gold Cluster Aggregation on TiO<sub>2</sub> via Surface Treatments, *J. Phys. Chem. C*, 2015, **119**, 24465–24474.

41 K. Nakata, S. Sugawara, W. Kurashige, Y. Negishi, M. Nagata, S. Uchida, C. Terashima, T. Kondo, M. Yuasa and A. Fujishima, Cossensitization Properties of Glutathione-Protected Au<sub>25</sub> Cluster on Ruthenium Dye-Sensitized TiO<sub>2</sub> Photoelectrode, *Int. J. Photoenergy*, 2013, **2013**, 456583.

42 K. Katsiev, G. Harrison, Y. Al-Salik, G. Thornton and H. Idriss, Gold Cluster Coverage Effect on H<sub>2</sub> Production over Rutile TiO<sub>2</sub> (110), *ACS Catal.*, 2019, **9**, 8294–8305.

43 P. López-Caballero, A. W. Hauser and M. a. Pilar de Lara-Castells, Exploring the Catalytic Properties of Unsupported and TiO<sub>2</sub>-Supported Cu<sub>5</sub> Clusters: CO<sub>2</sub> Decomposition to CO and CO<sub>2</sub> Photoactivation, *J. Phys. Chem. C*, 2019, **123**, 23064–23074.

44 I. Hadjoub, T. Touam, A. Chelouche, M. Atoui, J. Solard, M. Chakaroun, A. Fischer, A. Boudrioua and L.-H. Peng, Post-deposition annealing effect on RF-sputtered TiO<sub>2</sub> thin-film properties for photonic applications, *Appl. Phys. A*, 2016, **122**, 78.

45 J. Daughtry, A. Alotabi, L. Howard-Fabretto and G. G. Andersson, Composition and Properties of RF-Sputter Deposited Titanium Dioxide Thin Films, *Nanoscale Adv.*, 2020, **3**, 1077–1086.

46 Y. Fukamori, M. König, B. Yoon, B. Wang, F. Esch, U. Heiz and U. Landman, Fundamental Insight into the Substrate-Dependent Ripening of Monodisperse Clusters, *ChemCatChem*, 2013, **5**, 3330–3341.

47 H. Jensen, A. Soloviev, Z. Li and E. G. Søgaard, XPS and FTIR investigation of the surface properties of different prepared titania nano-powders, *Appl. Surf. Sci.*, 2005, **246**, 239–249.

48 G. Krishnan, H. S. Al Qahtani, J. Li, Y. Yin, N. Eom, V. B. Golovko, G. F. Metha and G. G. Andersson, Investigation of Ligand-Stabilized Gold Clusters on Defect-Rich Titania, *J. Phys. Chem. C*, 2017, **121**, 28007–28016.

49 E. Wahlström, N. Lopez, R. Schaub, P. Thostrup, A. Rønnaug, C. Africh, E. Lægsgaard, J. Nørskov and F. Besenbacher, Bonding of Gold Nanoclusters to Oxygen Vacancies on Rutile TiO<sub>2</sub> (110), *Phys. Rev. Lett.*, 2003, **90**, 026101.

50 J. Sasaki, N. Peterson and K. Hoshino, Tracer impurity diffusion in single-crystal rutile (TiO<sub>2</sub>-x), *J. Phys. Chem. Solids*, 1985, **46**, 1267–1283.

51 M. Li, W. Hebenstreit, U. Diebold, A. M. Tyryshkin, M. K. Bowman, G. G. Dunham and M. A. Henderson, The influence of the bulk reduction state on the surface structure and morphology of rutile TiO<sub>2</sub> (110) single crystals, *J. Phys. Chem. B*, 2000, **104**, 4944–4950.

52 T. Sekiya, T. Yagisawa, N. Kamiya, D. Das Mulmi, S. Kurita, Y. Murakami and T. Kodaira, Defects in anatase TiO<sub>2</sub> single crystal controlled by heat treatments, *J. Phys. Soc. Jpn.*, 2004, **73**, 703–710.

53 V. E. Henrich, G. Dresselhaus and H. Zeiger, Observation of Two-Dimensional Phases Associated with Defect States on the Surface of TiO<sub>2</sub>, *Phys. Rev. Lett.*, 1976, **36**, 1335.

54 P. Lindan, N. Harrison, M. Gillan and J. White, First-principles spin-polarized calculations on the reduced and reconstructed TiO<sub>2</sub> (110) surface, *Phys. Rev. B: Condens. Matter Mater. Phys.*, 1997, **55**, 15919.

55 T. Komaya, A. T. Bell, Z. Wengsiek, R. Gronsky, F. Engelke, T. S. King and M. Pruski, The influence of metal-support interactions on the accurate determination of Ru dispersion for Ru/TiO<sub>2</sub>, *J. Catal.*, 1994, **149**, 142–148.

56 W. E. Kaden, W. A. Kunkel, F. S. Roberts, M. Kane and S. L. Anderson, CO adsorption and desorption on size-selected Pdn/TiO<sub>2</sub> (110) model catalysts: Size dependence of binding sites and energies, and support-mediated adsorption, *J. Chem. Phys.*, 2012, **136**, 204705.

57 E. T. Baxter, M.-A. Ha, A. C. Cass, H. Zhai, A. N. Alexandrova and S. L. Anderson, Diborane Interactions with Pt<sub>7</sub>/



Alumina: Preparation of Size-Controlled Borated Pt Model Catalysts, *J. Phys. Chem. C*, 2018, **122**, 1631–1644.

58 T. J. Gorey, B. Zandkarimi, G. Li, E. T. Baxter, A. N. Alexandrova and S. L. Anderson, Preparation of Size and Composition-Controlled Pt<sub>n</sub>Sn<sub>x</sub>/SiO<sub>2</sub> (n= 2, 4, 24) Bimetallic Model Catalysts Using Atomic Layer Deposition, *J. Phys. Chem. C*, 2019, **123**(26), 16194–16209.

59 F. S. Roberts, M. D. Kane, E. T. Baxter and S. L. Anderson, Oxygen activation and CO oxidation over size-selected Pt n/alumina/Re (0001) model catalysts: correlations with valence electronic structure, physical structure, and binding sites, *Phys. Chem. Chem. Phys.*, 2014, **16**, 26443–26457.

60 T. J. Gorey, Y. Dai, S. L. Anderson, S. Lee, S. Lee, S. Seifert and R. E. Winans, Selective growth of Al<sub>2</sub>O<sub>3</sub> on size-selected platinum clusters by atomic layer deposition, *Surf. Sci.*, 2020, **691**, 121485.

61 M. Fauré, C. Saccavini and G. Lavigne, New insight into a convenient base-promoted synthesis of Ru<sub>3</sub>(CO)<sub>12</sub>, *Chem. Commun.*, 2003, 1578–1579.

62 G. Li, B. Zandkarimi, A. C. Cass, T. J. Gorey, B. J. Allen, A. N. Alexandrova and S. L. Anderson, Sn-modification of Pt<sub>7</sub>/alumina model catalysts: Suppression of carbon deposition and enhanced thermal stability, *J. Chem. Phys.*, 2020, **152**, 024702.

63 W. E. Kaden, W. A. Kunkel and S. L. Anderson, Cluster size effects on sintering, CO adsorption, and implantation in Ir/SiO<sub>2</sub>, *J. Chem. Phys.*, 2009, **131**, 114701.

64 M. Aizawa, S. Lee and S. L. Anderson, Deposition dynamics and chemical properties of size-selected Ir clusters on TiO<sub>2</sub>, *Surf. Sci.*, 2003, **542**, 253–275.

65 A. Ruiz Puigdollers, P. Schlexer, S. Tosoni and G. Pacchioni, Increasing oxide reducibility: the role of metal/oxide interfaces in the formation of oxygen vacancies, *ACS Catal.*, 2017, **7**, 6493–6513.

66 G. Pacchioni and H. Freund, Electron transfer at oxide surfaces. The MgO paradigm: from defects to ultrathin films, *Chem. Rev.*, 2013, **113**, 4035–4072.

67 T. Ueckert, R. Lamber, N. Jaeger and U. Schubert, Strong metal support interactions in a Ni/SiO<sub>2</sub> catalyst prepared via sol-gel synthesis, *Appl. Catal., A*, 1997, **155**, 75–85.

68 E. L. Strein and D. Allred, Eliminating carbon contamination on oxidized Si surfaces using a VUV excimer lamp, *Thin Solid Films*, 2008, **517**, 1011–1015.

69 D. J. Morgan, Resolving ruthenium: XPS studies of common ruthenium materials, *Surf. Interface Anal.*, 2015, **47**, 1072–1079.

70 Y. Zhang, J. R. Evans and S. Yang, Corrected values for boiling points and enthalpies of vaporization of elements in handbooks, *J. Chem. Eng. Data*, 2011, **56**, 328–337.

71 B. Zandkarimi, T. J. Gorey, G. Li, J. Munarriz, S. L. Anderson and A. N. Alexandrova, Alloying with Sn Suppresses Sintering of Size-Selected Sub-Nano Pt Clusters on SiO<sub>2</sub> with and without Adsorbates, *Chem. Mater.*, 2020, **32**, 8595–8605.

72 E. T. Baxter, M.-A. Ha, A. C. Cass, A. N. Alexandrova and S. L. Anderson, Ethylene dehydrogenation on Pt<sub>4</sub>, *7*, 8 clusters on Al<sub>2</sub>O<sub>3</sub>: Strong cluster size dependence linked to preferred catalyst morphologies, *ACS Catal.*, 2017, **7**, 3322–3335.

73 Y. Dai, T. J. Gorey, S. L. Anderson, S. Lee, S. Lee, S. Seifert and R. E. Winans, Inherent size effects on XANES of nanometer metal clusters: size-selected platinum clusters on silica, *J. Phys. Chem. C*, 2017, **121**, 361–374.

74 L. Sutton, Tables of interatomic distances and configuration in molecules and ions, *Chemical Society*, 1965, 10.

75 S. Labich, E. Taglauer and H. Knözinger, Metal-support interactions on rhodium model catalysts, *Top. Catal.*, 2000, **14**, 153–161.

76 S. Lee, C. Fan, T. Wu and S. L. Anderson, CO oxidation on Au n/TiO<sub>2</sub> catalysts produced by size-selected cluster deposition, *J. Am. Chem. Soc.*, 2004, **126**, 5682–5683.

77 R. White, T. Bennett, V. Golovko, G. G. Andersson and G. F. Metha, A Systematic Density Functional Theory Study of the Complete De-ligation of Ru<sub>3</sub>(CO)<sub>12</sub>, *ChemistrySelect*, 2016, **1**, 1163–1167.

78 D. P. Anderson, J. F. Alvino, A. Gentleman, H. A. Qahtani, L. Thomsen, M. I. J. Polson, G. F. Metha, V. B. Golovko and G. G. Andersson, Chemically-synthesised, atomically-precise gold clusters deposited and activated on titania, *Phys. Chem. Chem. Phys.*, 2013, **15**, 3917.

79 H. S. Al Qahtani, R. Higuchi, T. Sasaki, J. F. Alvino, G. F. Metha, V. B. Golovko, R. Adnan, G. G. Andersson and T. Nakayama, Grouping and aggregation of ligand protected Au<sub>9</sub> clusters on TiO<sub>2</sub> nanosheets, *RSC Adv.*, 2016, **6**, 110765–110774.

80 D. P. Anderson, R. H. Adnan, J. F. Alvino, O. Shipper, B. Donoeva, J.-Y. Ruzicka, H. A. Qahtani, H. H. Harris, B. Cowie, J. B. Aitken, V. B. Golovko, G. F. Metha and G. G. Andersson, Chemically synthesised atomically precise gold clusters deposited and activated on titania. Part II, *Phys. Chem. Chem. Phys.*, 2013, **15**, 14806.

81 Y. Kitsudo, A. Iwamoto, H. Matsumoto, K. Mitsuhashi, T. Nishimura, M. Takizawa, T. Akita, Y. Maeda and Y. Kido, Final state effect for Au 4f line from gold-nanoparticles grown on oxides and HOPG supports, *Surf. Sci.*, 2009, **603**, 2108–2114.

82 D.-C. Lim, C.-C. Hwang, G. Ganterföör and Y. D. Kim, Model catalysts of supported Au nanoparticles and mass-selected clusters, *Phys. Chem. Chem. Phys.*, 2010, **12**, 15172–15180.

83 C. C. Chusuei, X. Lai, K. Davis, E. Bowers, J. P. Fackler and D. Goodman, A nanoscale model catalyst preparation: Solution deposition of phosphine-stabilized gold clusters onto a planar TiO<sub>2</sub> (110) support, *Langmuir*, 2001, **17**, 4113–4117.

84 C. Vayenas, S. Brosda and C. Pliangos, The double-layer approach to promotion, electrocatalysis, electrochemical promotion, and metal-support interactions, *J. Catal.*, 2003, **216**, 487–504.

85 T. Ioannides and X. E. Verykios, Charge transfer in metal catalysts supported on doped TiO<sub>2</sub>: a theoretical approach based on metal–semiconductor contact theory, *J. Catal.*, 1996, **161**, 560–569.



86 L. Mezey and J. Giber, The surface free energies of solid chemical elements: calculation from internal free enthalpies of atomization, *Jpn. J. Appl. Phys.*, 1982, **21**, 1569.

87 Y. D. Kim, S. Schwegmann, A. P. Seitsonen and H. Over, Epitaxial growth of RuO<sub>2</sub> (100) on Ru (1010): Surface structure and other properties, *J. Phys. Chem. B*, 2001, **105**, 2205–2211.

88 A. Navrotsky, C. Ma, K. Lillova and N. Birkner, Nanophase transition metal oxides show large thermodynamically driven shifts in oxidation-reduction equilibria, *Science*, 2010, **330**, 199–201.

89 D. R. Lide, *CRC handbook of chemistry and physics: a ready-reference book of chemical and physical data*, CRC press, 1995.

90 L. Wang, T. Maxisch and G. Ceder, Oxidation energies of transition metal oxides within the GGA+ U framework, *Phys. Rev. B: Condens. Matter Mater. Phys.*, 2006, **73**, 195107.

91 E. Hebenstreit, W. Hebenstreit, H. Geisler, C. Ventrice Jr, P. Sprunger and U. Diebold, Bulk-defect dependent adsorption on a metal oxide surface: S/TiO<sub>2</sub> (110), *Surf. Sci.*, 2001, **486**, L467–L474.

92 F. Pesty, H.-P. Steinrück and T. E. Madey, Thermal stability of Pt films on TiO<sub>2</sub> (110): evidence for encapsulation, *Surf. Sci.*, 1995, **339**, 83–95.

93 Y. Gao, Y. Liang and S. Chambers, Thermal stability and the role of oxygen vacancy defects in strong metal support interaction—Pt on Nb-doped TiO<sub>2</sub> (100), *Surf. Sci.*, 1996, **365**, 638–648.

94 O. Dulub, W. Hebenstreit and U. Diebold, Imaging cluster surfaces with atomic resolution: the strong metal-support interaction state of Pt supported on TiO<sub>2</sub> (110), *Phys. Rev. Lett.*, 2000, **84**, 3646.

95 H. R. Sadeghi and V. E. Henrich, Rh on TiO<sub>2</sub>: Model catalyst studies of the strong metal-support interaction, *Appl. Surf. Sci.*, 1984, **19**, 330–340.

96 H. R. Sadeghi and V. E. Henrich, Electronic interactions in the rhodium/TiO<sub>2</sub> system, *J. Catal.*, 1988, **109**, 1–11.

97 Q. Fu and T. Wagner, Metal/oxide interfacial reactions: Oxidation of metals on SrTiO<sub>3</sub> (100) and TiO<sub>2</sub> (110), *J. Phys. Chem. B*, 2005, **109**, 11697–11705.

98 A. Howard, C. Mitchell, D. Morris, R. Egddell and S. Parker, The surface structure of TiO<sub>2</sub> (210) studied by atomically resolved STM and atomistic simulation, *Surf. Sci.*, 2000, **448**, 131–141.

99 R. Bennett, P. Stone and M. Bowker, Pd nanoparticle enhanced re-oxidation of non-stoichiometric TiO<sub>2</sub>: STM imaging of spillover and a new form of SMSI, *Catal. Lett.*, 1999, **59**, 99–105.

100 D. Mullins and K. Zhang, Metal–support interactions between Pt and thin film cerium oxide, *Surf. Sci.*, 2002, **513**, 163–173.

101 S. Tauster, S. Fung and R. L. Garten, Strong metal-support interactions. Group 8 noble metals supported on titanium dioxide, *J. Am. Chem. Soc.*, 1978, **100**, 170–175.

102 S. Tauster, S. Fung, R. Baker and J. Horsley, Strong interactions in supported-metal catalysts, *Science*, 1981, **211**, 1121–1125.

103 G. L. Haller and D. E. Resasco, Metal–support interaction: Group VIII metals and reducible oxides, *Advances in catalysis*, Elsevier, 1989, pp. 173–235.

104 S. Bernal, F. Botana, J. Calvino, C. López, J. Pérez-Omil and J. Rodríguez-Izquierdo, High-resolution electron microscopy investigation of metal–support interactions in Rh/TiO<sub>2</sub>, *J. Chem. Soc., Faraday Trans.*, 1996, **92**, 2799–2809.

105 S. Bernal, J. Calvino, M. Cauqui, J. Gatica, C. L. Cartes, J. P. Omil and J. Pintado, Some contributions of electron microscopy to the characterisation of the strong metal–support interaction effect, *Catal. Today*, 2003, **77**, 385–406.

106 T. Sham, T. Ohta, T. Yokoyama, Y. Kitajima, M. Funabashi, N. Kosugi and H. Kuroda, Ru L edge x-ray absorption studies of the electronic structure of Ru<sub>3</sub>(CO)<sub>12</sub> adsorption and the formation of Ru–Cu bimetallics on Cu (111), *J. Chem. Phys.*, 1988, **88**, 475–477.

107 H. Feng, J. Lu, P. C. Stair and J. W. Elam, Alumina over-coating on Pd nanoparticle catalysts by atomic layer deposition: enhanced stability and reactivity, *Catal. Lett.*, 2011, **141**, 512–517.

108 W. Kurashige, R. Kumazawa, D. Ishii, R. Hayashi, Y. Niihori, S. Hossain, L. V. Nair, T. Takayama, A. Iwase, S. Yamazoe, T. Tsukuda, A. Kudo and Y. Negishi, Au25-Loaded BaLa<sub>4</sub>Ti<sub>4</sub>O<sub>15</sub> Water-Splitting Photocatalyst with Enhanced Activity and Durability Produced Using New Chromium Oxide Shell Formation Method, *J. Phys. Chem. C*, 2018, **122**, 13669–13681.

109 S. Vajda, M. J. Pellin, J. P. Greeley, C. L. Marshall, L. A. Curtiss, G. A. Ballentine, J. W. Elam, S. Catillon-Mucherie, P. C. Redfern and F. Mehmood, Subnanometre platinum clusters as highly active and selective catalysts for the oxidative dehydrogenation of propane, *Nat. Mater.*, 2009, **8**, 213–216.

